

물분해 소재 합성 공정 최신전략

Synthetic Strategies of Water Splitting Catalysts/Materials

Uk Sim, Ph. D.

Research theme

Materials


- Nanoparticle/nanomaterial synthesis using CVD, hydro-, solvo-thermal, electrospinning method, ...
- Thermoelectric materials
- Carbon-based Catalysts (Graphene, GQDs, ...)
- Bio-inspired Materials
- Conducting polymer
- Metal-doped TiO₂ based Photocatalysts
- Metal Carbide/Nitride/Phosphide/Sulfide Materials
- Surface / interface treatment by ALD
- 3D Printing-based Materials Design
- Single-Atomic Catalysts

Applications


- Photoelectrochemistry/ Electrochemistry
- Water splitting reaction (OER, HER)
- Fuel Cell System (HOR, ORR)
- CO₂ reduction to Hydrocarbon Production
- Supercapacitor/Hybrid Capacitor
- Metal-Air Battery (Zn, Li, ...)
- Nitrogen Cycle such as N₂ Reduction, NH₃ Oxidation, NO²⁻/NO³⁻ reduction, NO_x reduction, ...
- Ammonia/VOC Decomposition
- Surface/Interface Tuning using Redox Mediator
- Functional Surfaces with Wettability Control
- Alcohol, Urea Oxidation in (Non)aqueous system

Mechanism and fundamental study

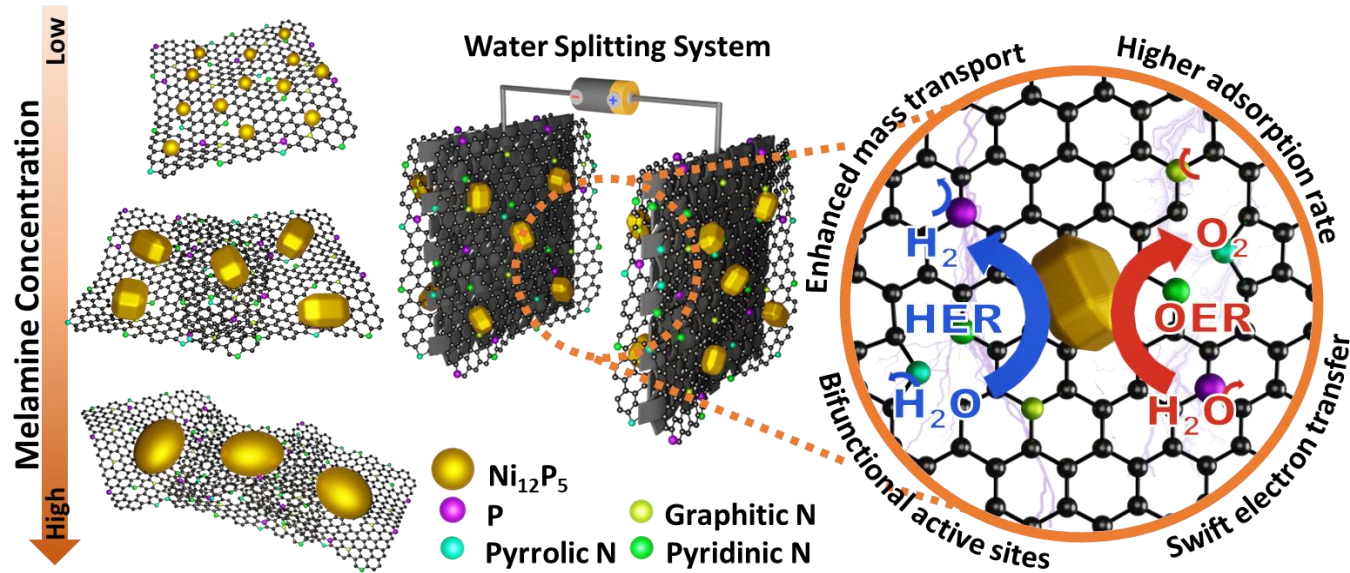
- In-depth electrochemical reaction study
- Atomic scale calculation using DFT
- Machine Learning-assisted Catalytic Materials



**Anchoring of Ni₁₂P₅ Micro-bricks
in Nitrogen and Phosphorus-rich
Carbon Framework: Engineering
Bifunctional Active Sites for
Efficient Water Splitting System**



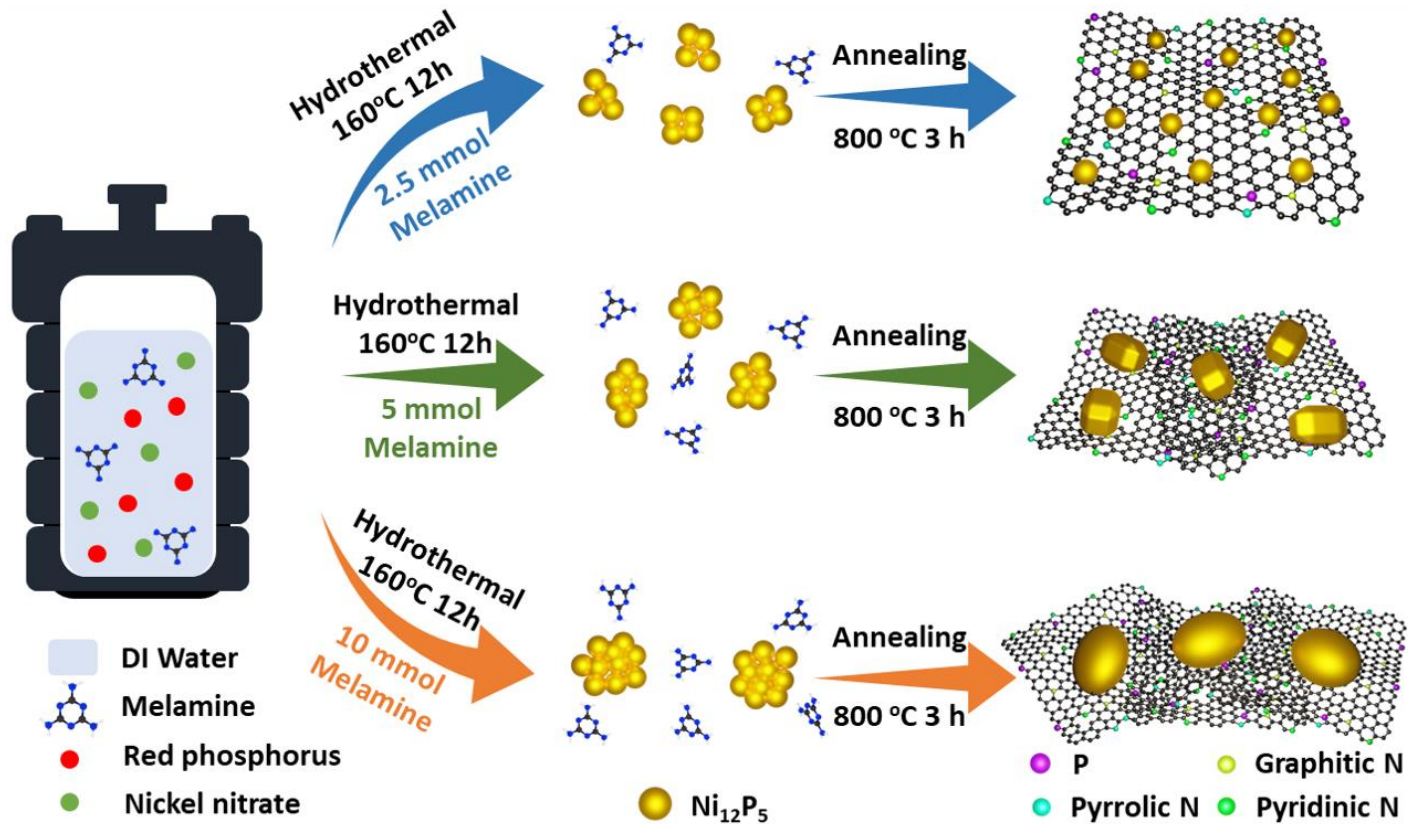
Design of an Effective Bifunctional Electrocatalyst



- Nickel phosphide is able to effectively weaken the Gibbs free energy of reactant adsorption (ΔG_{H^*}) on the surface of metal phosphides, which is beneficial for fast hydrogen evolution. In general, OER is easier to occur in alkaline electrolytes, while HER more easily goes on in acid electrolytes. Nevertheless, P-rich precious MPs have both superior HER and OER activities in alkaline electrolytes, thus appropriate as bifunctional catalysts to achieve highly efficient overall water splitting and provide a feasible strategy to solve the energy problems in the future.
- Nevertheless, compared to P-lean materials, P-rich ones usually have poorer conductivity due to with more phosphorus-phosphorus and metal-phosphorus bonds and less metal-metal bonds, thus requiring some additional strategies, such as carbon modification, element doping and loading on the conductive substrates, to further improve the conductivity.
- Hence, we aim to modify the physical structure, surface nature, and decorated the Ni_{12}P_5 particles in the carbon network to create the ample number of active centers for bifunctional electrocatalytic activities based on simple experimental protocols.
- Morphological evolution of Ni_{12}P_5 with a variation in the melamine concentration ranging from 2.5 to 10 mmol.

Preparation of Ni₁₂P₅@N,P-C electrocatalysts

- This study focuses on distinct Ni₁₂P₅ microbricks in nitrogen- and phosphorus-rich carbon matrices; these matrices are developed using a facile hydrothermal-*followed* pyrolysis treatment to explore their bifunctional activity in a water-splitting system.



- The engineered surface morphology and fine-tuned three-way active centers (Ni (δ^+), P (δ^-), and pyridinic N/graphitic N) improved the kinetic rate and resilient durability of the Ni₁₂P₅@N,P-C(5) microbricks.

X-Ray-Diffraction and Photoelectron Spectroscopy

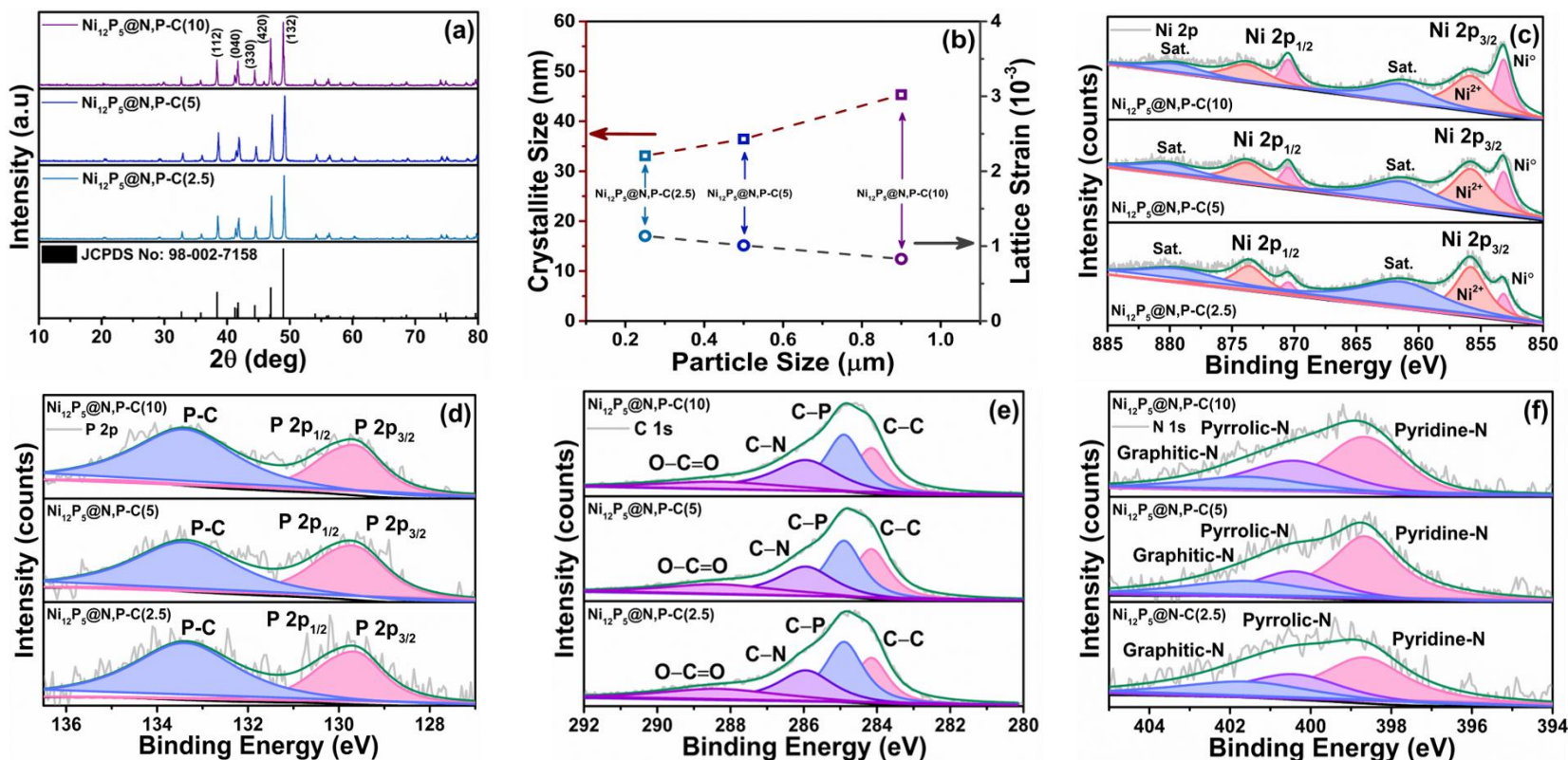


Figure 1. (a) XRD patterns, (b) calculated crystallite size, particle size, and lattice strain values, (c) Ni 2p, (d) P 2p, (e) C 1s, and (f) N 1s XPS spectra of prepared $\text{Ni}_{12}\text{P}_5@N,P-C$ samples, respectively.

- Tetragonal crystal structure. Crystallite size of 2.5, 5, and 10 samples were calculated 33.10, 36.44, and 45.33 nm. Lattice strain is observed to gradually decrease with respect to the grain size.
- Grain boundaries restricts the better conductivity.
- Observed $\text{Ni}^{\delta+}$, $\text{P}^{\delta-}$ and nitrogen and phosphorous in the carbon network (XPS) plays the influential role during electrochemical reactions.

Morphology and Microstructure analysis

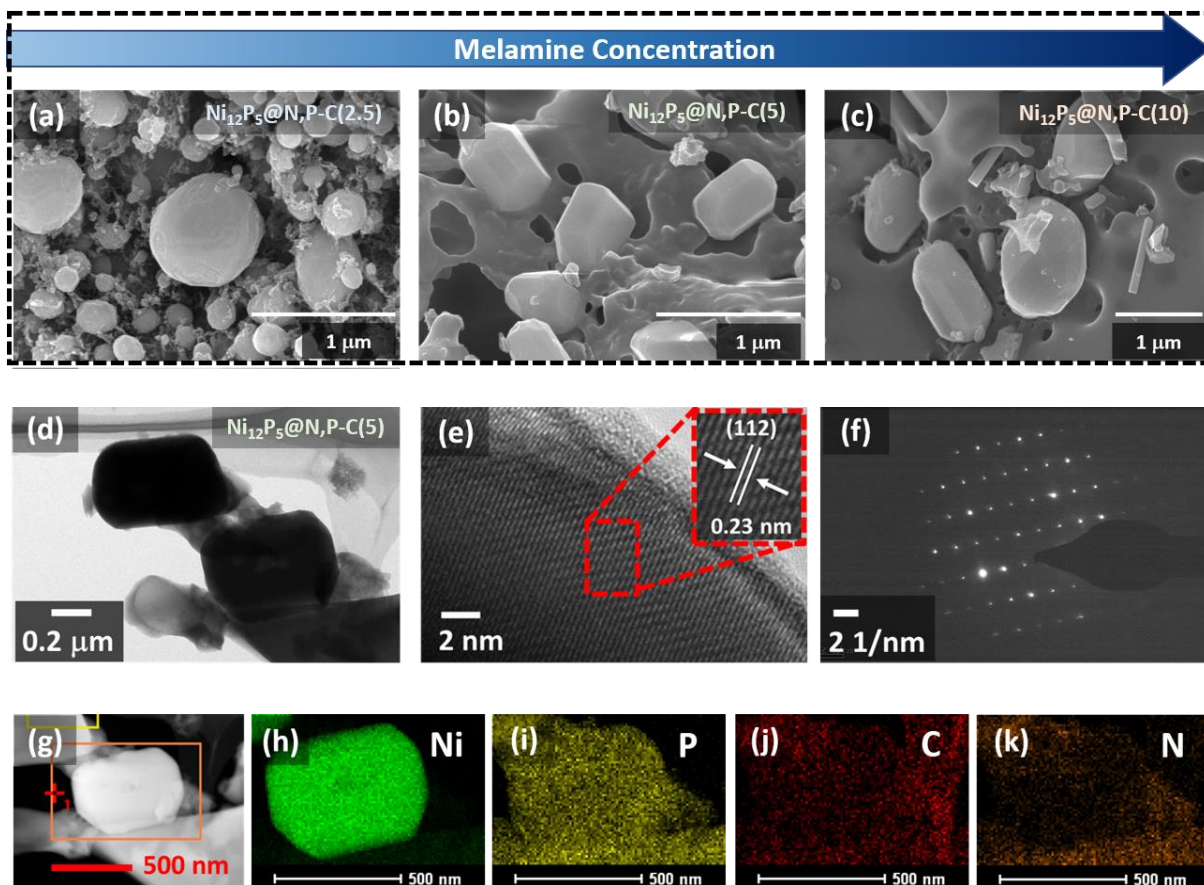


Figure 2. (a-c) FESEM images of $\text{Ni}_{12}\text{P}_5@N,P-C$ electrocatalysts corresponding to the increase in melamine concentration. (d-e) Low magnification TEM image, (e) HRTEM image (inset: interplanar spacing) (f) SAED pattern, and (g-k) Elemental mapping images of $\text{Ni}_{12}\text{P}_5@N,P-C(5)$, respectively.

At 5 mmol concentration of melamine, Nickel phosphide forms the Microbricks of $\text{Ni}_{12}\text{P}_5@N,P-C(5)$

- ✓ Microbricks lattice fringes with an inter-planar spacing of 0.23 nm to the d-spacing of (112) crystal plane of Ni_{12}P_5 structure.
- ✓ EDS-maps Displays the presence and distribution of Ni, P, C, and N elements in the $\text{Ni}_{12}\text{P}_5@N,P-C(5)$. Further, validate the doping of excess P and N in the carbon structure.
- ✓ Thus, the prepared control samples well agree with the synthesis condition.

Oxygen Evolution Reaction

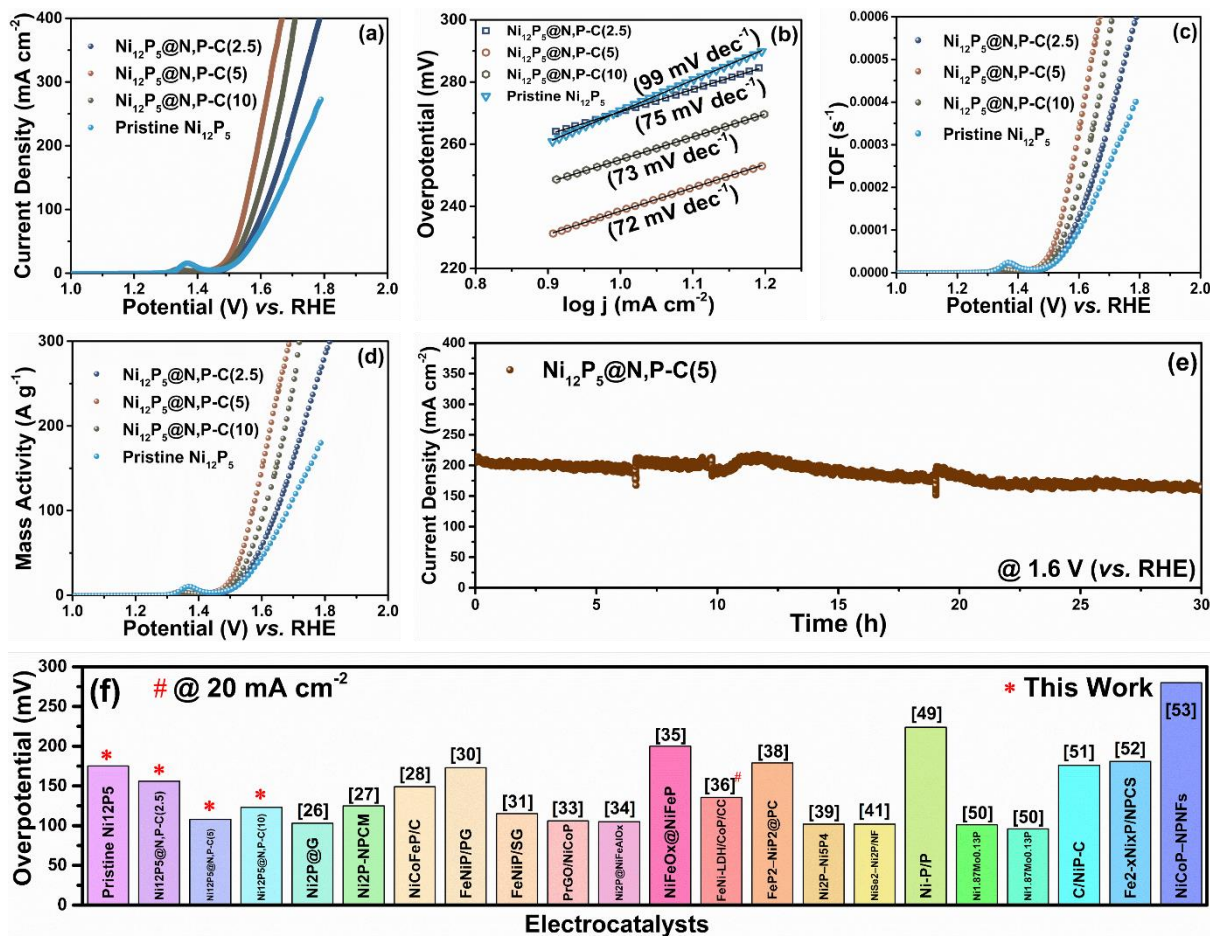


Figure 3. (a) OER polarization curves, (b) Tafel slope, (c) TOF, and (d) mass activity of prepared Ni₁₂P₅@N,P-C samples, respectively, (e) OER CA curve of Ni₁₂P₅@N,P-C(5) and (f) the comparison chart of the prepared Ni₁₂P₅@N,P-C samples with respect to the reported electrocatalysts.

- Comparatively, Ni₁₂P₅@N,P-C(5) generates an early OER onset potential at 1.46 V (vs. RHE) and enforces a low OER overpotential of 229 mV to attain a current density of 10 mA cm⁻². Its less Tafel slope indicates the improved kinetics.
- High values of MA and TOF of Ni₁₂P₅@N,P-C(5) helped to attain the better OER activity.
- The observed CA curve indicates the strong durability of the Ni₁₂P₅@N,P-C(5) electrocatalysts for OER activity in a highly alkaline environment.

Hydrogen Evolution Reaction

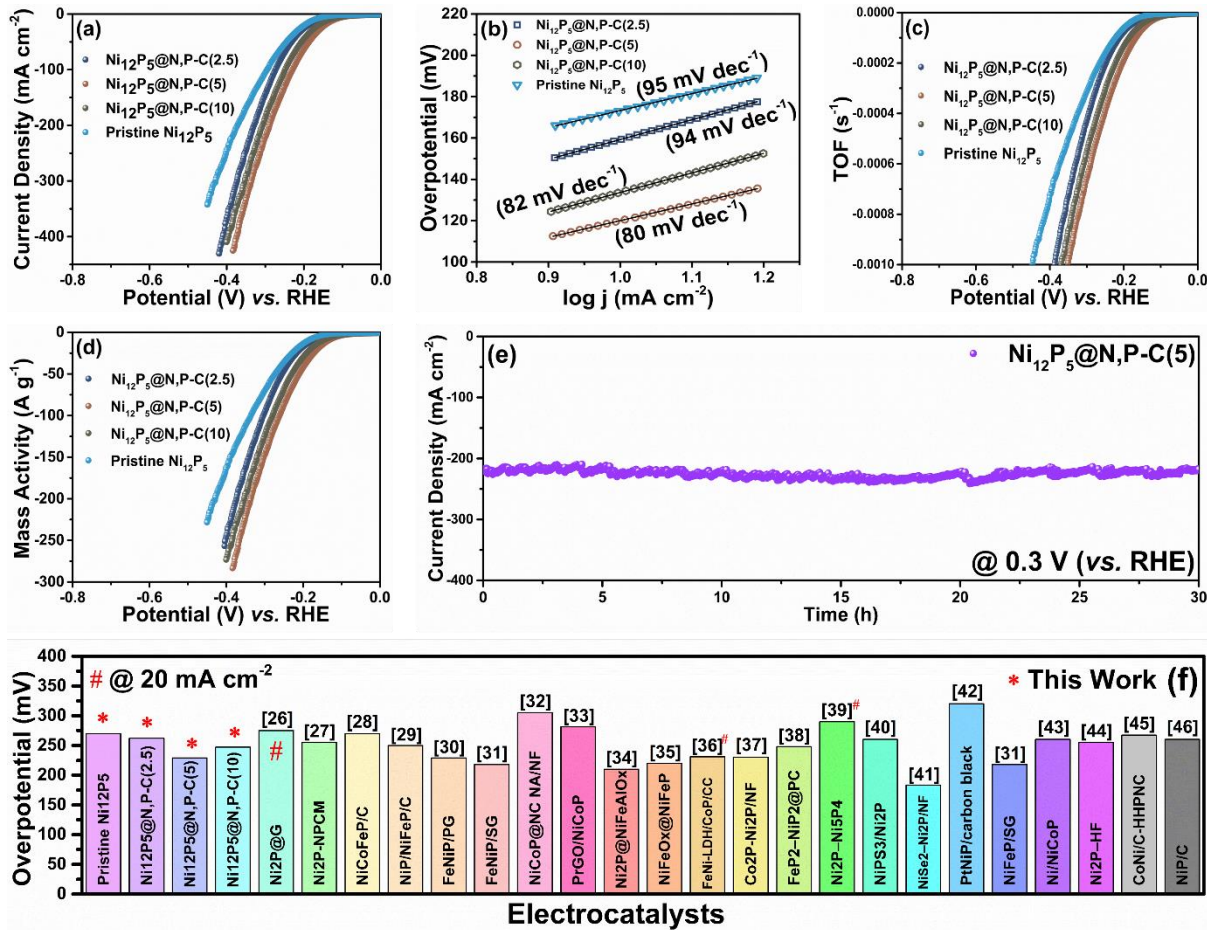


Figure 4. (a) HER polarization curves, (b) Tafel slope, (c) TOF, and (d) mass activity of prepared Ni₁₂P₅@N,P-C samples, respectively, (e) HER CA curve of Ni₁₂P₅@N,P-C(5),

- Ni₁₂P₅@N,P-C(5) with a low HER overpotential value of 108 mV compared with those of Ni₁₂P₅@N,P-C(2.5) (156 mV), Ni₁₂P₅@N,P-C(10) (123 mV), and pristine Ni₁₂P₅ (175 mV), to drive a current density of 10 mA cm⁻².
- Based on the Tafel slope value (80), it has been assumed that Ni₁₂P₅@N,P-C(5) follows the Volmer–Heyrovsky mechanism in HER.
- High values of MA and TOF of Ni₁₂P₅@N,P-C(5) helped to attain the better HER activity.
- Observed CA curve indicates the strong durability of the Ni₁₂P₅@N,P-C(5) electrocatalysts for HER activity in a highly alkaline environment.

Electrochemical analysis

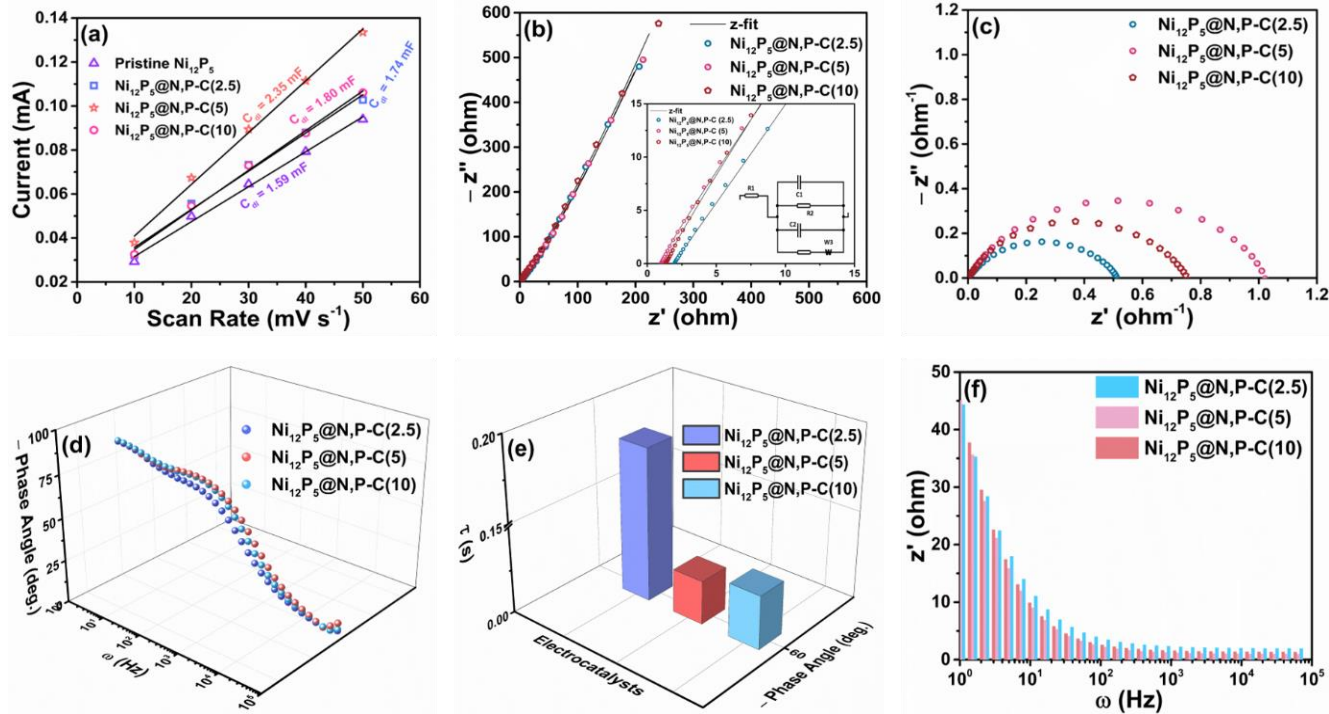


Figure 5. (a) ECSA curves, (b) Nyquist impedance plot, (c) Nyquist admittance plot, (d) Bode's plot, (e) Calculated relaxation time, and (f) z' vs. frequency plot of prepared $\text{Ni}_{12}\text{P}_5@N,P-C$ samples, respectively.

- The obtained C_{dl} values reveals the ECSA of $\text{Ni}_{12}\text{P}_5@N,P-C(2.5)$ is higher than the other electrocatalysts.
- The relatively low R_s and R_{ct} values of $\text{Ni}_{12}\text{P}_5@N,P-C(5)$ from Nyquist plot ensure relatively rapid kinetics of the interfacial charge transfer reaction.
- In Nyquist admittance plot, semicircle of $\text{Ni}_{12}\text{P}_5@N,P-C(5)$ is larger than that of the others, indicating the boosted kinetics of the interfacial charge transfer reaction.
- The time constant is calculated from the Bode plot and found that there is lesser value for $\text{Ni}_{12}\text{P}_5@N,P-C(5)$. This indicates the time taken by the adsorption of the intermediates is relatively shorter in $\text{Ni}_{12}\text{P}_5@N,P-C(5)$.

Electrochemical water splitting

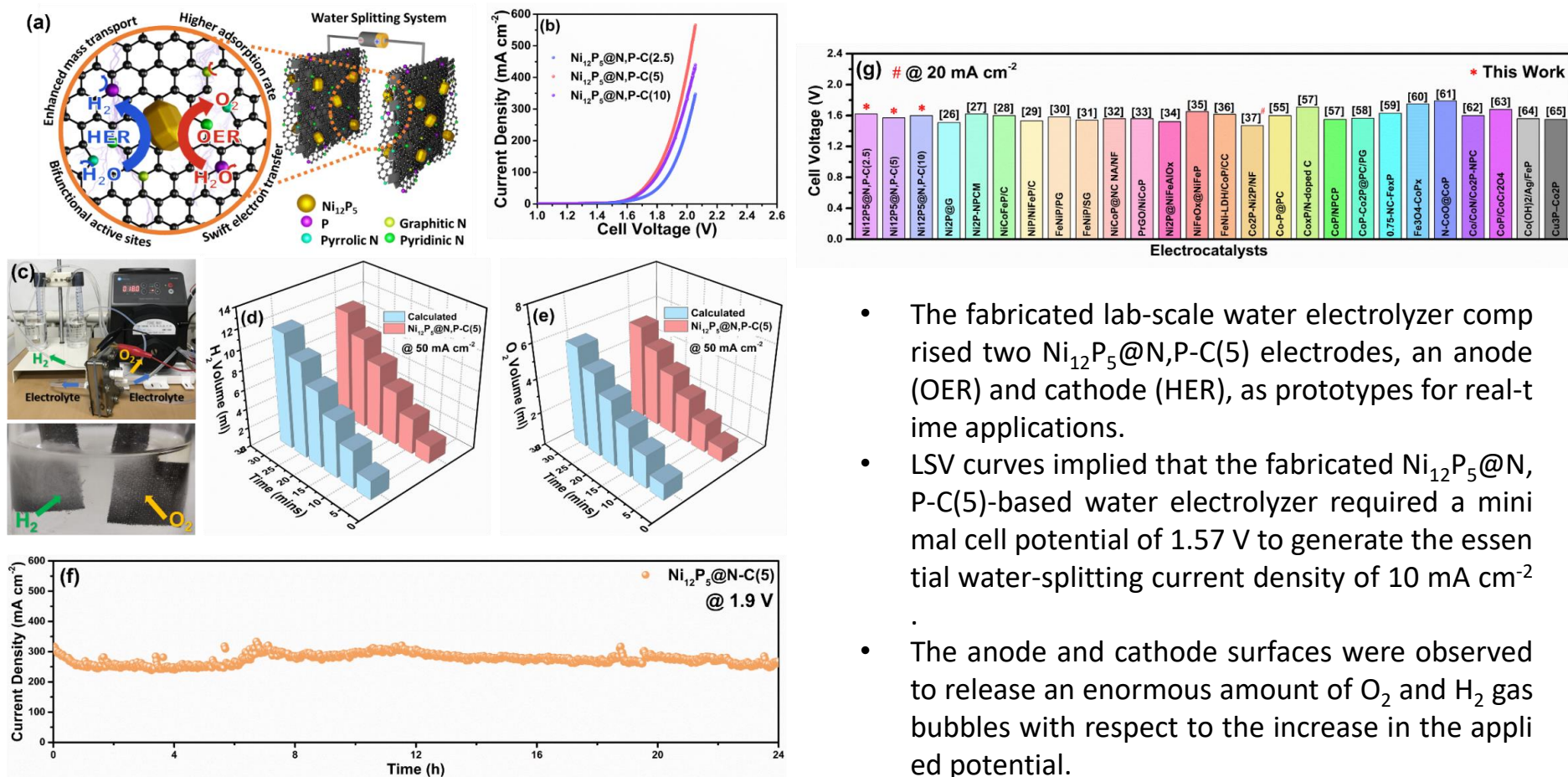


Figure 6. (a) Scheme representing bifunctional activities in $\text{Ni}_{12}\text{P}_5@N,P-C(5)$, (b) LSV curves of $\text{Ni}_{12}\text{P}_5@N,P-C$ based water splitting system, (c) CA curve of $\text{Ni}_{12}\text{P}_5@N,P-C(5)$ water splitting system and (f) the comparison chart of the prepared $\text{Ni}_{12}\text{P}_5@N,P-C$ samples with respect to the reported electrocatalysts.

- The fabricated lab-scale water electrolyzer comprised two $\text{Ni}_{12}\text{P}_5@N,P-C(5)$ electrodes, an anode (OER) and cathode (HER), as prototypes for real-time applications.
- LSV curves implied that the fabricated $\text{Ni}_{12}\text{P}_5@N,P-C(5)$ -based water electrolyzer required a minimal cell potential of 1.57 V to generate the essential water-splitting current density of 10 mA cm^{-2} .
- The anode and cathode surfaces were observed to release an enormous amount of O_2 and H_2 gas bubbles with respect to the increase in the applied potential.
- The long-term operation of $\text{Ni}_{12}\text{P}_5@N,P-C(5)$ in a water electrolyzer was tested at 0.3 V vs. RHE, which showed its stable and effective water-splitting activity for 10 h.

Enhanced Bifunctional Electrocatalytic Activity of Ni-Co Bimetallic Chalcogenides for an Efficient Overall Water Splitting Application

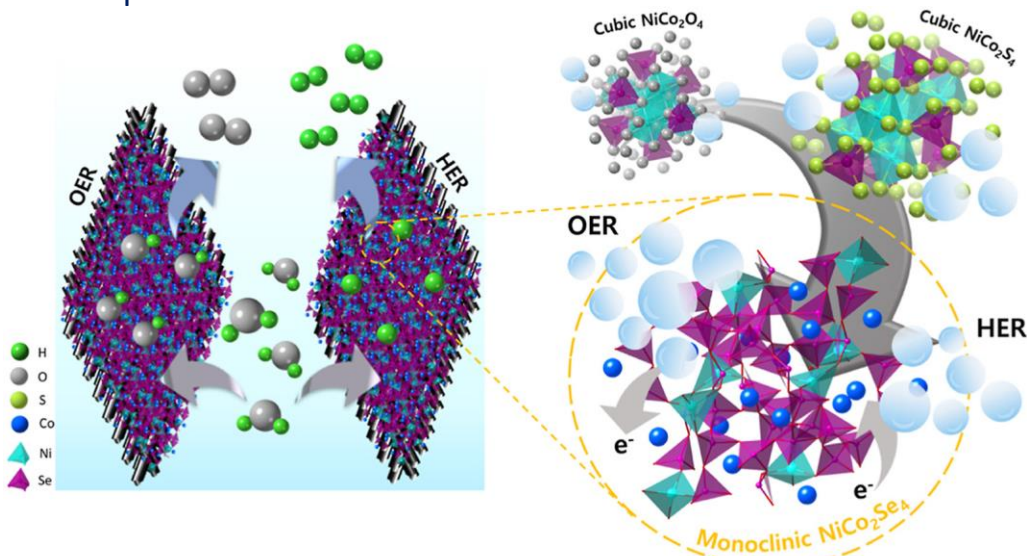
Published

Gnanaprakasam Janani, Subramanian Yuvaraj,
Subramani Surendran, Yujin Chae, Yelyn Sim, Sun-Ju Song,
Woosung Park *, Myoung-Jin Kim *, Uk Sim*

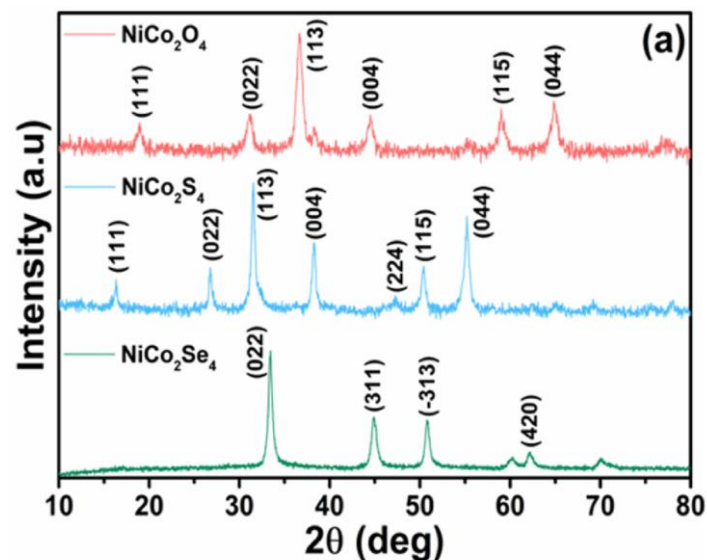
Ni-Co Bimetallic Chalcogenides for Water Splitting

Journal of Alloys and Compounds (2020) 156389

➤ Graphical abstract



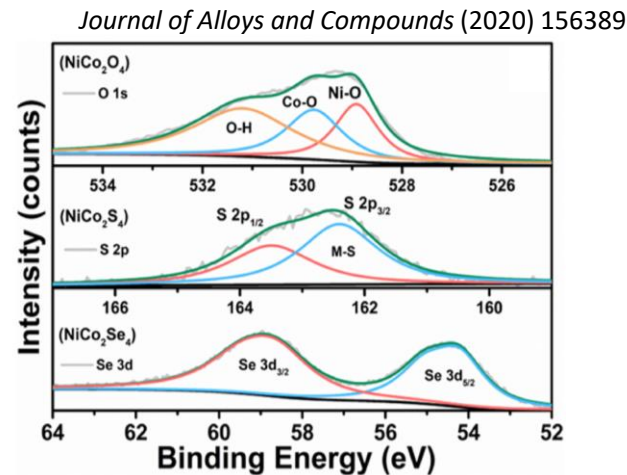
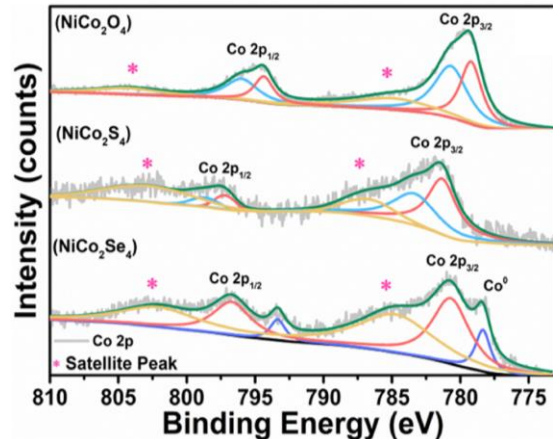
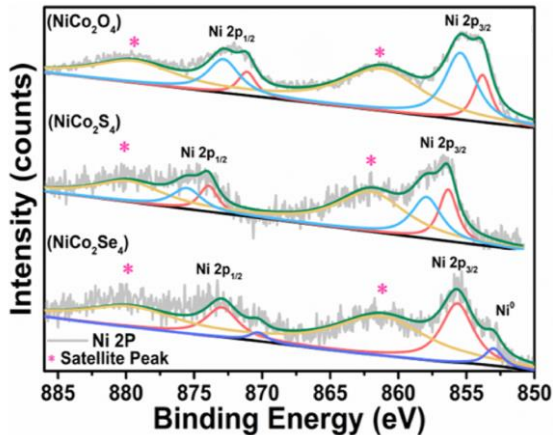
➤ XRD pattern



- The XRD patterns shown in Figure (a) indicate that pure phases of NiCo₂O₄, NiCo₂S₄, and NiCo₂Se₄ were formed with unique crystal structures.
- Well-defined and intense peaks were observed at 36.705°, 64.964°, and 31.152° for NiCo₂O₄ and 31.459°, 55.082°, and 38.168° for NiCo₂S₄, which were indexed to the 113, 044, and 022 and 113, 044, and 004 planes of the cubic crystal structure with calculated cell parameters $a = b = c = 8.1140 \text{ \AA}$ and 9.4240 \AA , corresponding to the JCPDS cards of NiCo₂O₄ (98-002-4211) and NiCo₂S₄ (98-062-4467), respectively.
- Similarly, the peaks observed at 33.296°, 44.788°, 50.786°, and 62.101° for NiCo₂Se₄ were indexed to the 002, 311, -313, and 420 planes of the monoclinic crystal structure with calculated cell parameters $a = 11.99 \text{ \AA}$, $b = 3.54 \text{ \AA}$, and $c = 6.09 \text{ \AA}$ corresponding to the JCPDS card of NiCo₂Se₄ (81-4821).
- XRD patterns measured for the three prepared samples are in good agreement with the standard data and display no impurities.

Ni-Co Bimetallic Chalcogenides for Water Splitting

➤ XPS spectra

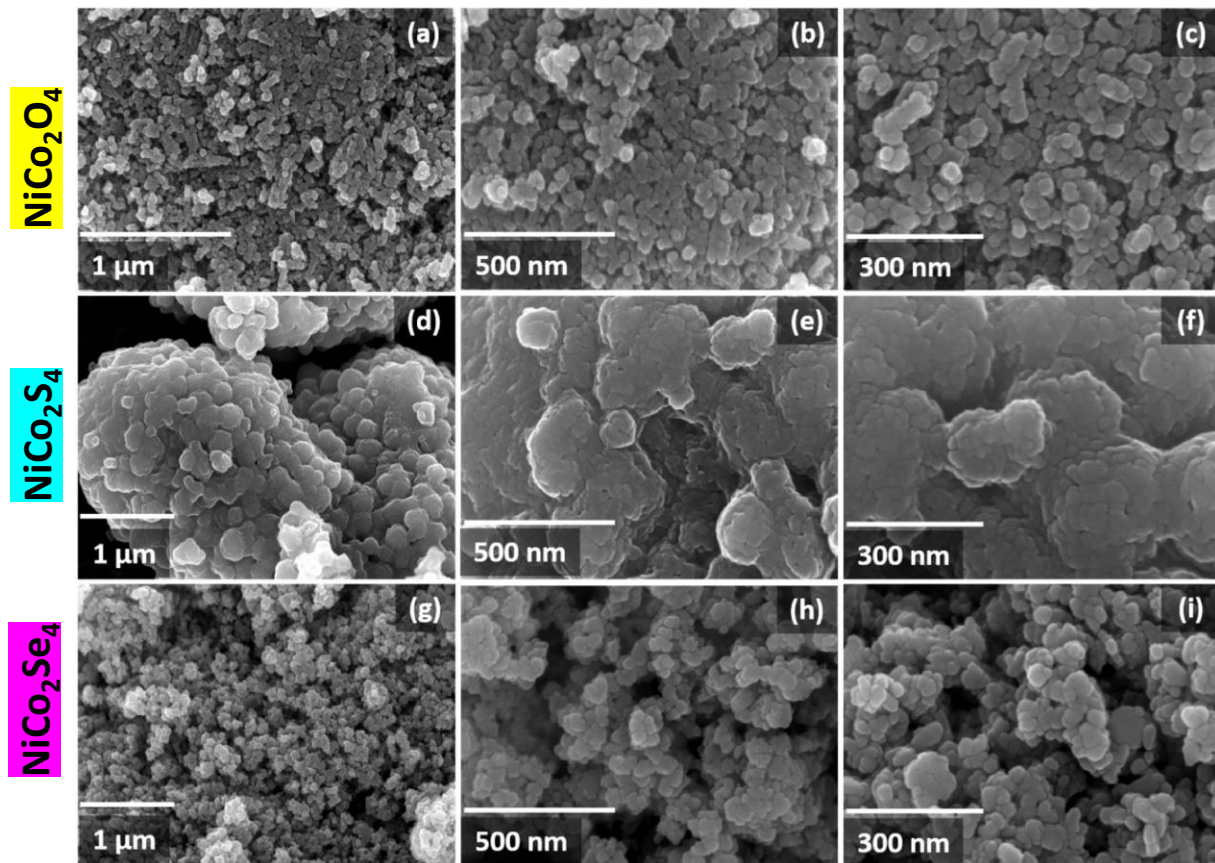


- Ni 2p XPS spectrum shown in Fig. (b) shows prominent peaks corresponding to the Ni 2p_{3/2} and Ni 2p_{1/2} spin-orbital splitting of Ni in NiCo₂O₄, NiCo₂S₄, and NiCo₂Se₄.
- The Ni 2p peaks observed at binding energies of **853.82 eV** and **855.48 eV** in NiCo₂O₄ and **856.34 eV** and **858.04 eV** in NiCo₂S₄ are ascribed to the Ni²⁺ and Ni³⁺ oxidation states, which correspond to Ni-O and Ni-S bonding, respectively.
- Ni 2p spectrum for NiCo₂Se₄ shows the characteristic metallic Ni peak at **853.00 eV**, which was found to be absent in the NiCo₂O₄ and NiCo₂S₄ samples. (This is attributed to the presence of partially charged Ni (Ni^{δ+}, δ ≥ 0)).
- The Ni 2p_{3/2} and Ni 2p_{1/2} peaks at **855.67 eV** and **873.32 eV** are attributed to the Ni²⁺ state assigned to the Ni-Se bond, with a consistent shakeup satellite peak at 861.30 eV .
- Fig.(c) displays a **metallic peak** at **778.33 eV**, which is consistent with the Ni 2p spectrum, highlighting the metallic properties of NiCo₂Se₄.
- From Fig. (d), Ni-O and Co-O peaks are observed at 528.91 eV and 529.76 eV, respectively, along with a surface O-H peak at 531.22 eV, whereas the S 2p spectra for NiCo₂S₄ and NiCo₂Se₄ reveal that the 2p_{3/2} and 2p_{1/2} peaks for S at 162.41 eV and 163.49 eV can be attributed to Ni-S and Co-S bonds, respectively.
- Presence of Ni^{2+,3+} and Co^{2+,3+} mixed-valence states in NiCo₂O₄, and NiCo₂S₄, respectively. In contrast, NiCo₂Se₄ has a metallic nature with Ni^{0+,2+} and Co^{0+,2+} valence states, which have a beneficial role in electrocatalytic activity.

Ni-Co Bimetallic Chalcogenides for Water Splitting

➤ FE-SEM Images

Journal of Alloys and Compounds (2020) 156389



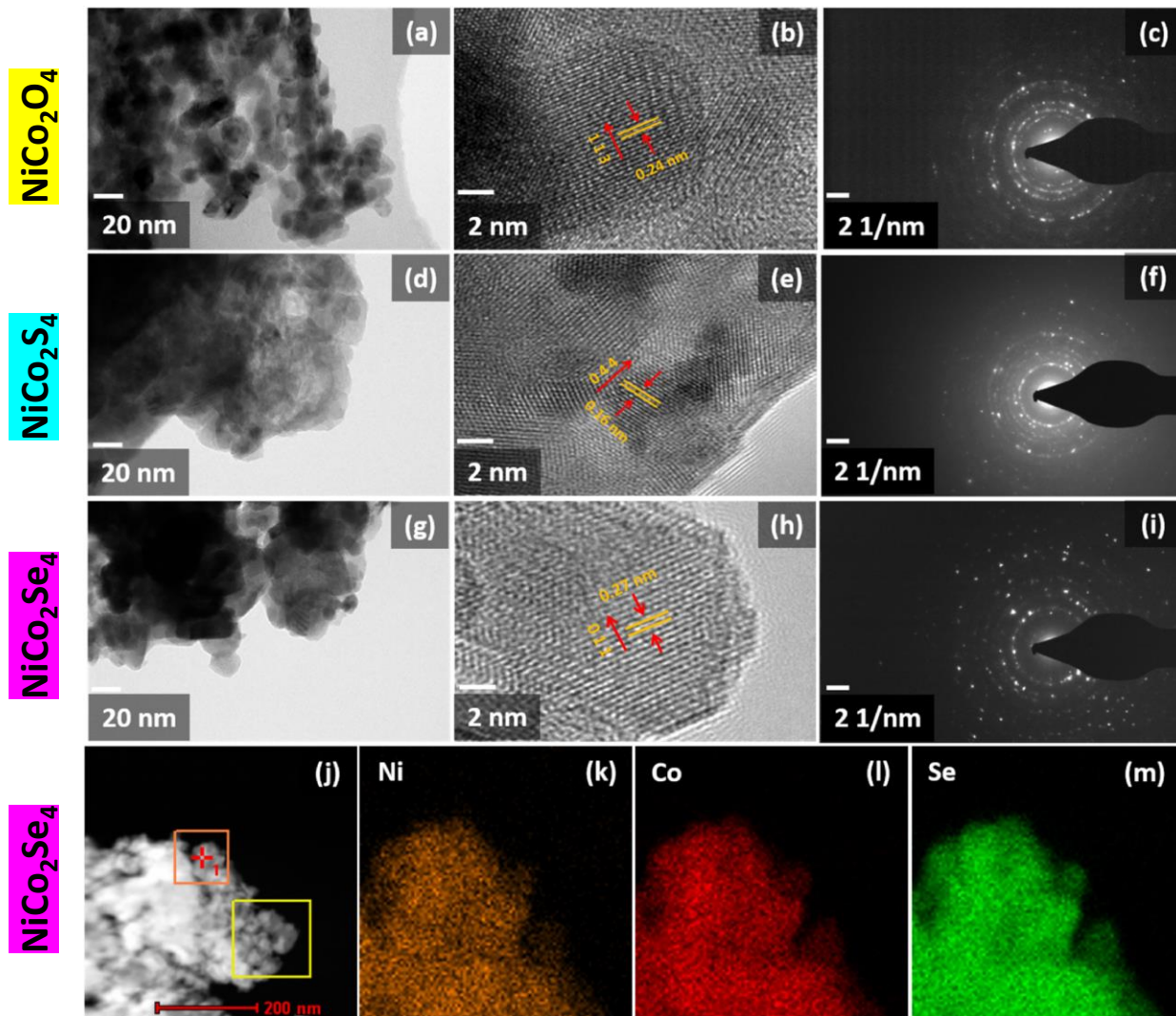
- Fig. 2(a–c) display clusters of nano-particles, which are uniformly distributed to form a nanostructure of porous-like voids that ease the transport of ions.
- Fig. 2(d–f) shows uniformly fused nanostructures of NiCo₂S₄ nano-particles, with a larger particle size distribution than that found for the NiCo₂O₄ nanoparticles.
- The NiCo₂S₄ nanoparticles show an improved surface roughness that enhances the absorption of electrolytic ions.

- In Fig. 2(g–i), the NiCo₂Se₄ nano-particles are observed in clusters similar to the NiCo₂O₄ nanoparticles, with a higher degree of pore-like voids.
- Thus, the morphology of the NiCo₂Se₄ nanostructures enhances the electrocatalytic activity of the material compared to that of the NiCo₂O₄ and NiCo₂S₄ nanostructures.

Ni-Co Bimetallic Chalcogenides for Water Splitting

➤ HRTEM Images & SAED patterns & Elemental mapping Images

Journal of Alloys and Compounds (2020) 156389

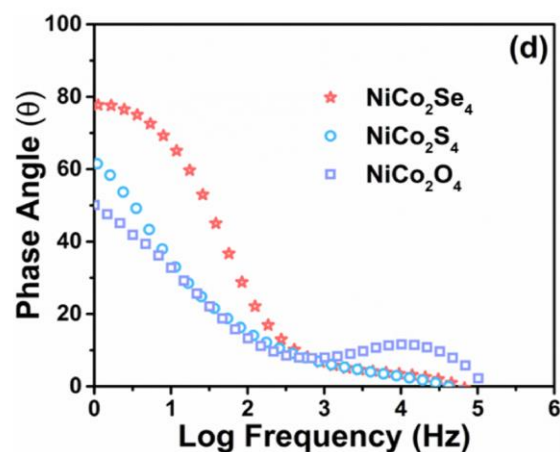
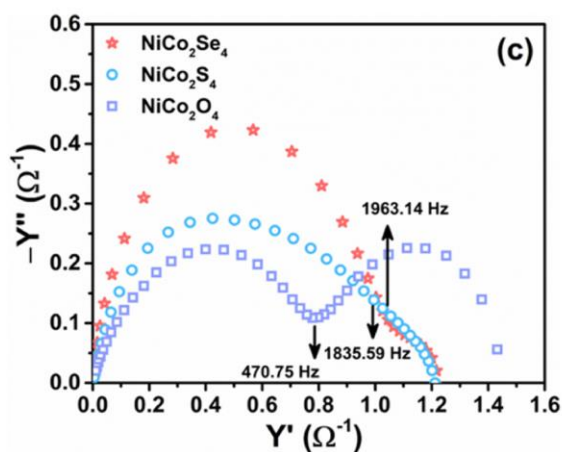
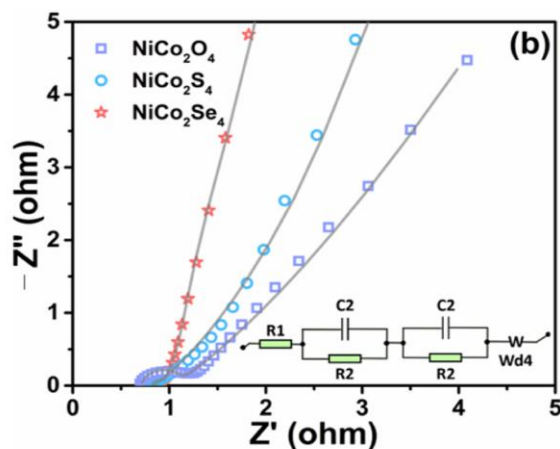
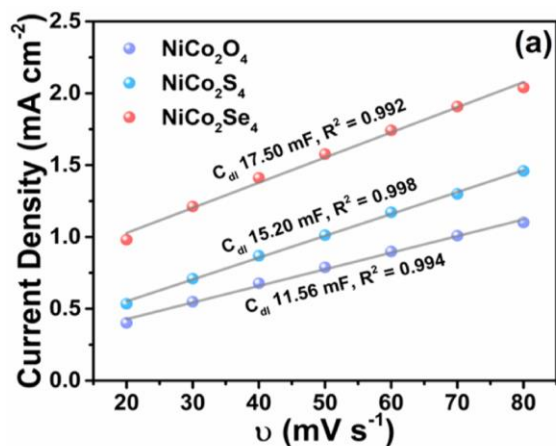


- In Fig. (a), (d), and (g) evidence distinct lattice fringes, which have an interplanar spacing of 0.24 nm, 0.16 nm, and 0.27 nm, corresponding to the (113), (044), and (002) planes.
- Fig. (c), (f), and (i) show the SAED patterns related to the lattice fringes of the prepared NiCo_2O_4 , NiCo_2S_4 , and NiCo_2Se_4 nanostructures, respectively, evidencing their polycrystalline nature.
- In Fig. (j–m) show uniformly distributed signals for Ni, Co, and Se in the NiCo_2Se_4 sample.
- The analysis confirms that the constitutional elements are uniformly distributed throughout the prepared NiCo_2Se_4 nanostructures.

Ni-Co Bimetallic Chalcogenides for Water Splitting

EIS analysis

Journal of Alloys and Compounds (2020) 156389

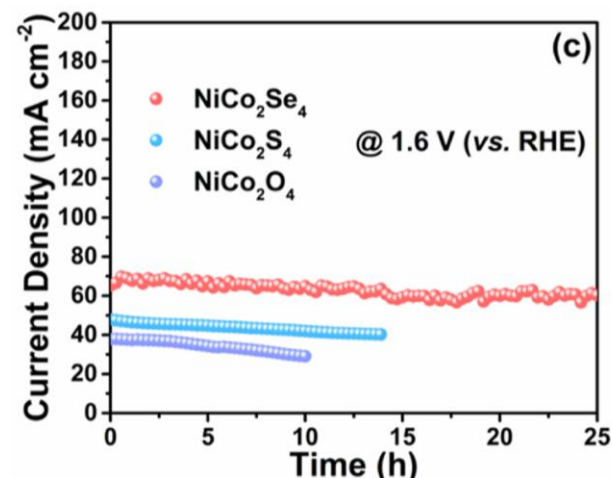
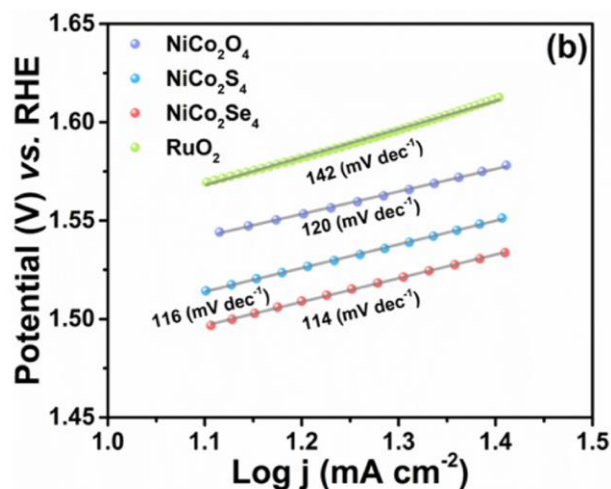
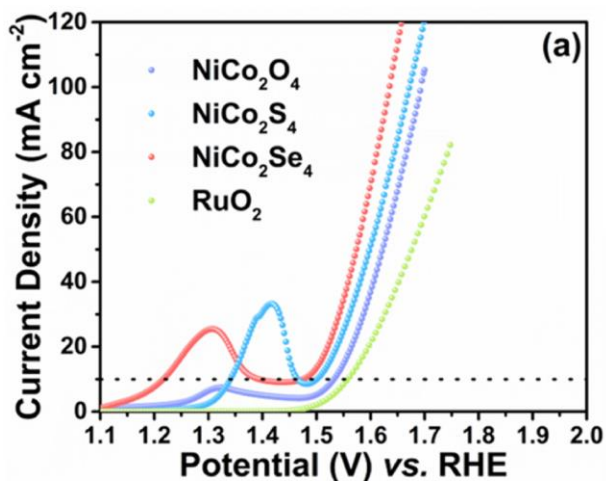


- As shown in Fig. (a), the measured charging currents were fitted by linear regression with respect to the scan rates to obtain C_{dl} .
 - Shown in Fig. (b), Nyquist plot displays a semicircle in the high-frequency region.
 - Nyquist admittance plot in Fig. (c) reveals a high knee frequency of 1963 Hz, 1835 Hz, and 470.75 Hz for the NiCo₂Se₄, NiCo₂S₄, and NiCo₂O₄ electrodes, respectively.
 - The higher knee frequency found for the NiCo₂Se₄ electrode is due to its low charge transfer resistance, as shown in Fig. (b).
 - In Fig. (d) Bode admittance plot, a high-phase angle of 79° is observed for the NiCo₂Se₄ electrode, which linearly declines from the high-to low-frequency region, confirming the enhanced redox activity.
- From the Nyquist and Bode plots, it is evidenced that the NiCo₂Se₄ electrode exhibits improved electron transfer kinetics with respect to the NiCo₂O₄ and NiCo₂S₄ electrodes, strongly enhancing its electrocatalytic activity.

Ni-Co Bimetallic Chalcogenides for Water Splitting

Journal of Alloys and Compounds (2020) 156389

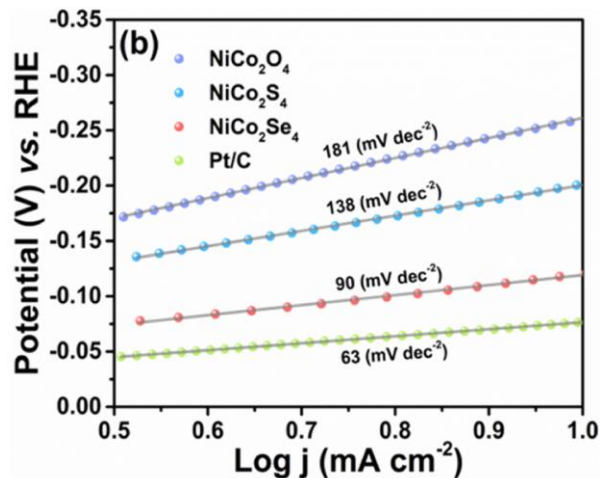
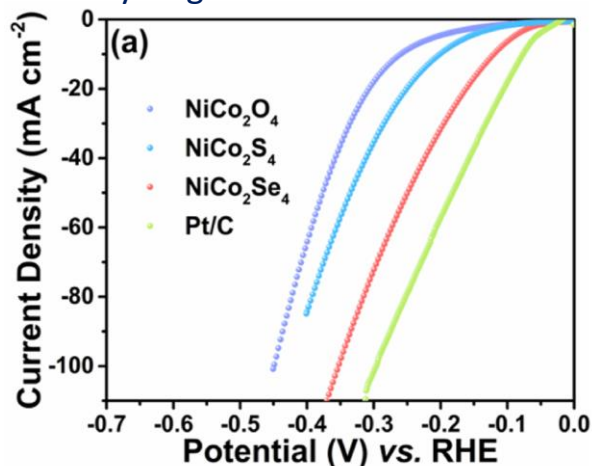
➤ Oxygen Evolution Reaction



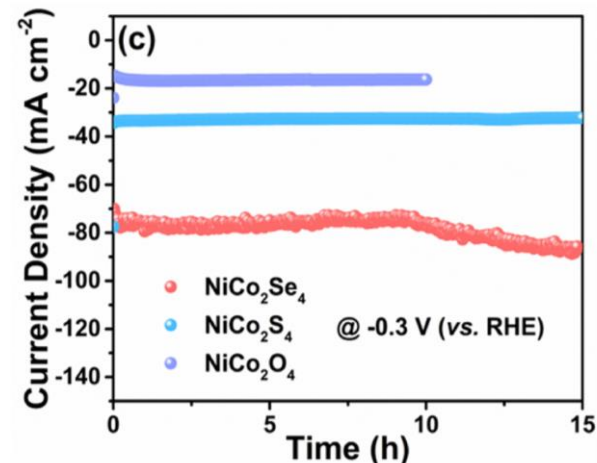
- The overpotential for the metallic NiCo₂Se₄ was determined to be **245 mV** (at a current density of 10 mA cm⁻²).
- This is 27 mV, 56 mV, and 83 mV lower than that found for the NiCo₂S₄ (272 mV), NiCo₂O₄ (301 mV), and RuO₂ (326 mV) electrocatalysts.
- NiCo₂Se₄ has low-valence Ni⁰⁺ and Co⁰⁺ states that serve as influential electroactive sites for the OER activity.
- The presence of metallic Ni and Co induces high electron transfer kinetics between the surface of the catalyst and the substrate.
- Metallic NiCo₂Se₄ electrocatalyst was identified as an efficient electrocatalyst that promotes the OER activity.
- In Fig. (c), OER durability of each electrocatalysts in aqueous electrolytes was measured for 25 h, 15 h, and 10 h, respectively, by chronoamperometry (CA) analysis at a constant potential of 1.6 V (vs. RHE).
- The metallic NiCo₂Se₄ generated a constant current density, confirming its stable durability.
- In contrast, the NiCo₂O₄ and NiCo₂S₄ electrocatalysts lost approximately **20%** of their initial current density, evidencing a lack of stability in aqueous electrolytes.

Ni-Co Bimetallic Chalcogenides for Water Splitting

Hydrogen Evolution Reaction



Journal of Alloys and Compounds (2020) 156389

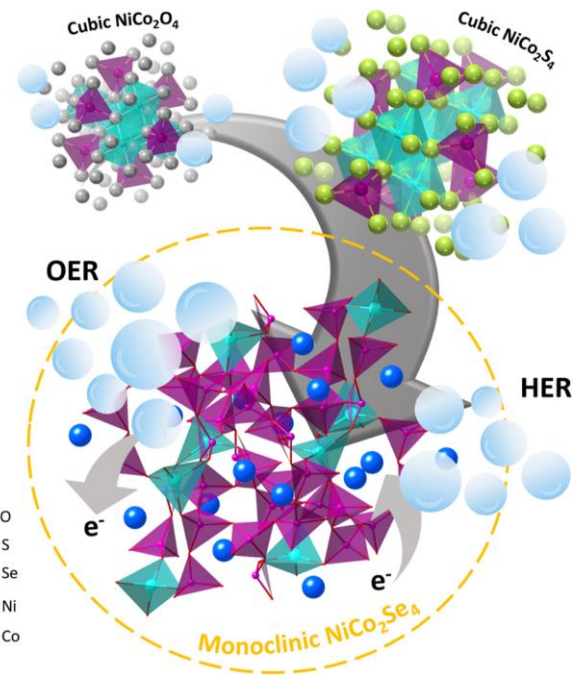
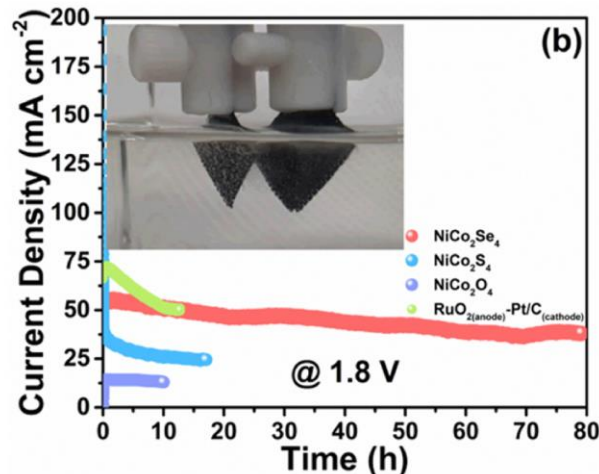
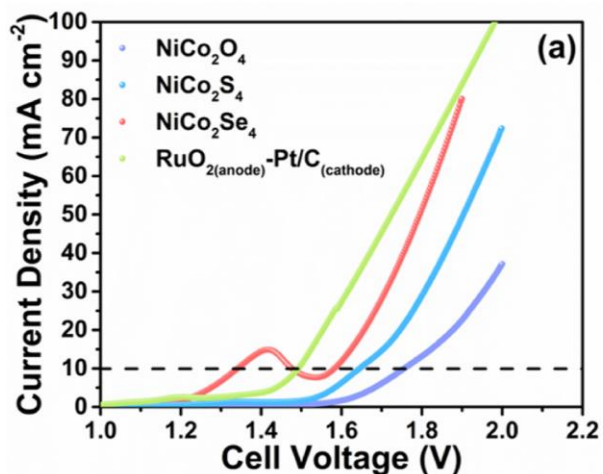


- The metallic NiCo₂Se₄ electrocatalyst showed an HER overpotential of **122 mV** at a current density of 10 mA cm⁻², significantly lower than that found for NiCo₂S₄ (202 mV) and NiCo₂O₄ (261 mV).
- Tafel slope of **90 mV dec⁻¹** is found for the NiCo₂Se₄ electrocatalyst, which is lower than that found for the NiCo₂S₄ (138 mV dec⁻¹) and NiCo₂O₄ (181 mV dec⁻¹) electrocatalysts.
- Rate-determining step of the NiCo₂Se₄ HER activity is the **hydrogen adsorption/discharge reaction**.
- HER durability of the NiCo₂O₄, NiCo₂S₄, and metallic NiCo₂Se₄ electrocatalysts was determined by carrying out CA measurements for approximately 15 h at a constant potential of -0.3 V (vs. RHE), as shown in Fig. (c).
- Metallic NiCo₂Se₄ revealed an improvement in the current density, owing to enhancement of surface-active sites due to low surface poisoning.
- Particle induces a pulverization effect that activates the electrocatalyst through exploitation of the native oxide layer, which, thereby, increases the effective surface area and number of active sites at the surface of the electrocatalyst.
- This confirms the durability and strength of the prepared metallic NiCo₂Se₄ electrocatalyst for HER activity in aqueous electrolytes.

Ni-Co Bimetallic Chalcogenides for Water Splitting

Fabrication of a lab-scale water-splitting system

Journal of Alloys and Compounds (2020) 156389



- The obtained LSV curves evidence that metallic NiCo₂Se₄ requires a minimum cell voltage of **1.58 V**, close to that found for the benchmark Pt/C/RuO₂ (1.49 V), to generate an optimal current of 10 mA.
- Instead, the NiCo₂O₄ (1.75 V) and NiCo₂S₄ (1.64 V) systems require a higher cell voltage to produce the same current.
- The fabricated RuO_{2(anode)}-Pt/C_(cathode), NiCo₂O₄, NiCo₂S₄, and metallic NiCo₂Se₄-based water-splitting systems were examined by CA (Fig. (b)) to measure their durability in a highly alkaline electrolyte.
- In all systems, the anode and cathode initiate the reactions of molecular oxygen and hydrogen at a standing cell voltage of 1.8 V, respectively.
- The metallic NiCo₂Se₄-based water-splitting system was maintained for approximately 80 h, whereas the RuO_{2(anode)}-Pt/C_(cathode), NiCo₂S₄ and NiCo₂O₄-based systems were maintained for only 15 h, 20 h and 10 h, respectively, indicating a constant decrease in current density in high alkaline condition.

$\text{Ni}_2\text{P}_2\text{O}_7$ microsheets as efficient Bi-functional electrocatalysts for water splitting application

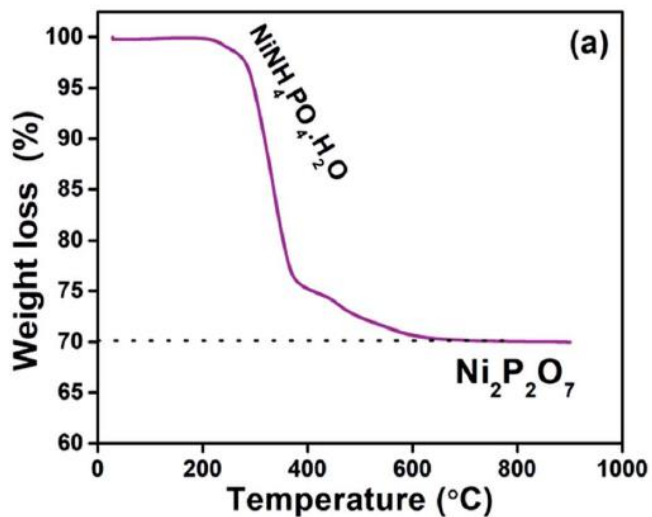
Published

Subramani Surendran ^{abc}, Arumugam Sivanantham ^b,
Sangaraju Shanmugam ^{*b}, Uk Sim ^{*c} and
Ramakrishnan Kalai Selvan ^{*a}

Ni₂P₂O₇ Microsheets for Water Splitting

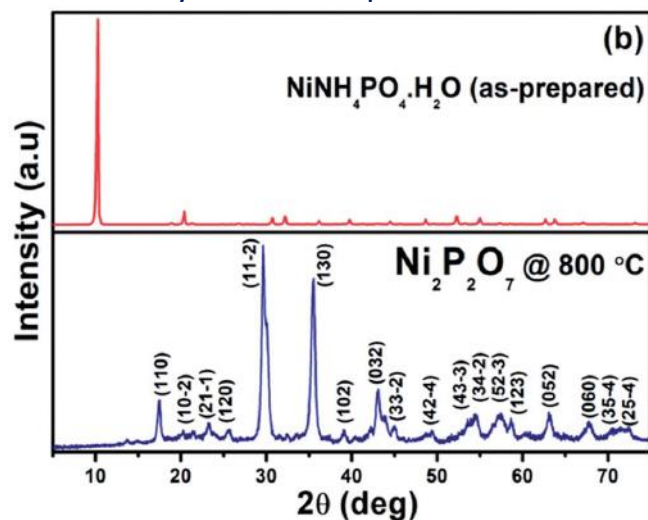
Sustainable Energy Fuels, 2019,3, 2435-2446

➤ TGA curve



- From the TGA curve, a continuous weight loss of about 30% was observed from room temperature to 700 °C.
- The constant weight loss may be due to the presence of excess hydroxyl and amino groups in the material.
- After the exclusion of the unstable compositions, the sample became stable at around 700 °C.
- At 800 °C, a more thermally stable and highly crystalline sample was obtained.

➤ X-ray diffraction patterns

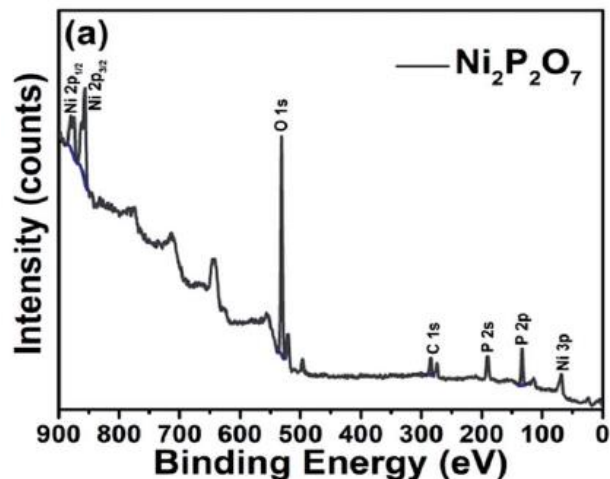


- Interestingly, the obtained high-intensity diffraction peaks at 17.55°, 29.97°, 35.45° and 43.12°, corresponding to the $(h k l)$ planes of (110), (11-2), (130) and (032), respectively, well matched with single phase Ni₂P₂O₇ (JCPDS card no. 00-039-071).
- The obtained diffraction peaks further illustrate the formation of a phase pure monoclinic crystal system of Ni₂P₂O₇ with a space group of $P2_1/c$ (space group number 14).

Ni₂P₂O₇ Microsheets for Water Splitting

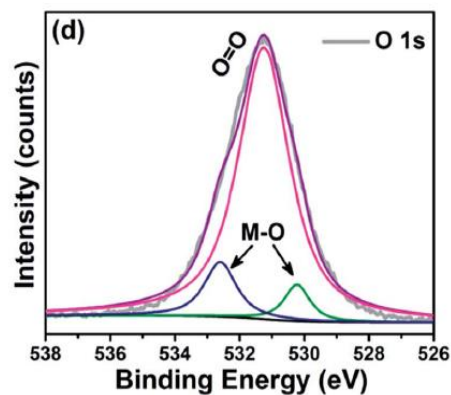
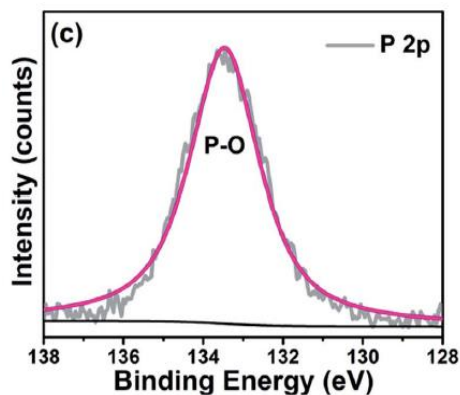
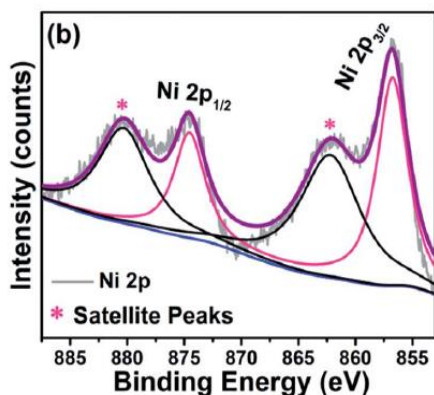
Sustainable Energy Fuels, 2019,3, 2435-2446

➤ Survey scan X-ray Photoelectron Spectroscopy spectra



- Fig. 2(a) displays the wide survey spectrum of the Ni₂P₂O₇ sample, which reveals the existence of Ni 2p, P 2p, and O 1s elements in the sample.
- From the XPS spectrum, the composition of the elements was determined to be 22.04 at% of Ni, 20.85 at% of P, and 57.1 at% of O, confirming the equal distribution of the elements in the surface.

➤ Ni 2p, P 2p, O 1s X-ray Photoelectron Spectroscopy spectra

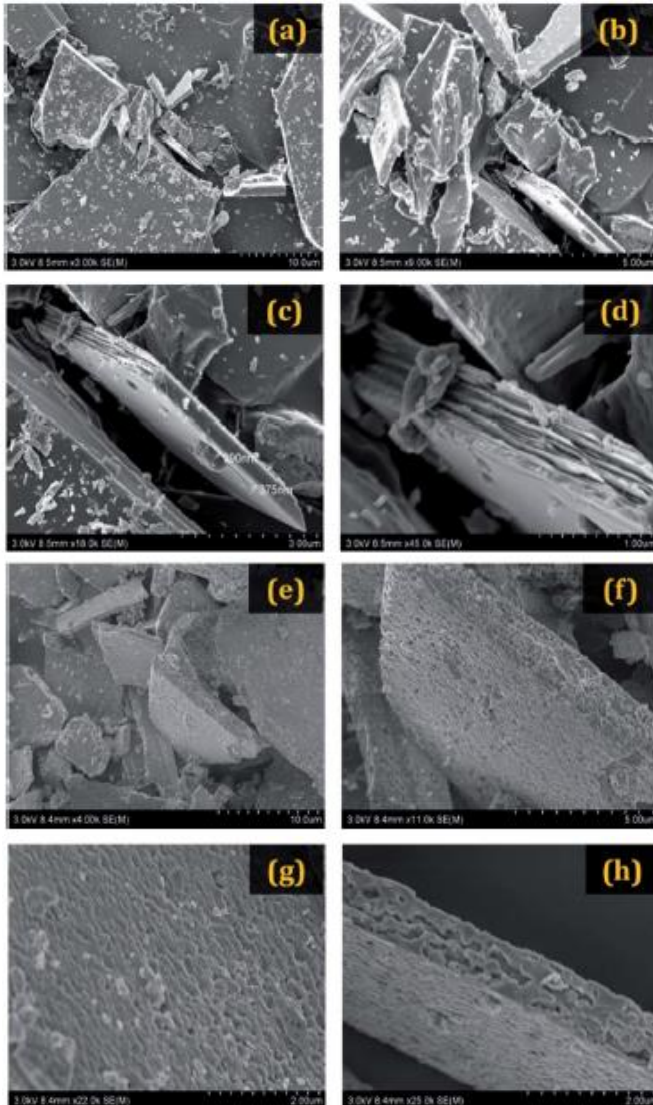


- Hence, the XPS results confirm the presence of the required elements in relation to the theoretical value of Ni₂P₂O₇.

Ni₂P₂O₇ Microsheets for Water Splitting

Sustainable Energy Fuels, 2019,3, 2435-2446

➤ Scanning Electron Microscopy (SEM) images

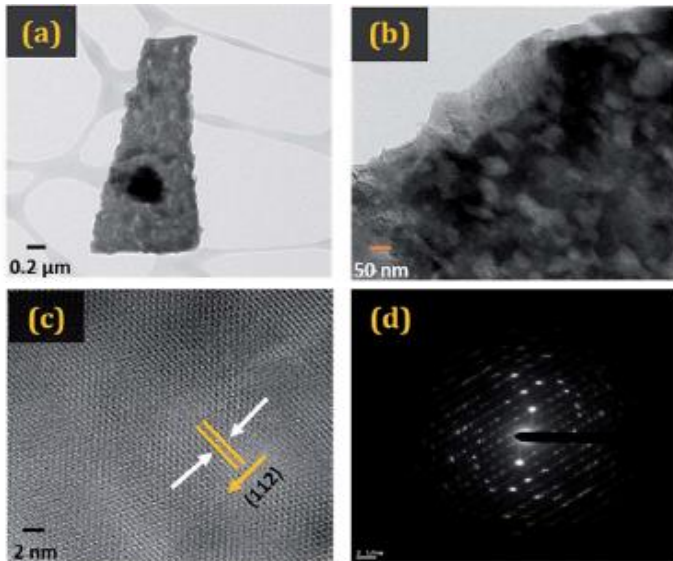


- The SEM images of the as prepared sample in Figure (a–d) display the shattered sheets of the nanostructured material.
- The cross-sectional view indicates that the samples are made up of layered nanosheets, stacked densely one over the other.
- The thickness of the closely stacked sheet was estimated to be around 400 nm with its length stretching from 1–3 mm.
- The calcinated Ni₂P₂O₇ not only retained the **microsheet structure**, but also advantageously generated surface alteration to create **spongy, porous microstructures** of Ni₂P₂O₇.
- This porous nature was realized to be uniformly distributed in all the shattered sheets of Ni₂P₂O₇.
- The established consistently spread spongy, porous microstructures can offer an enhanced roughness factor that constructively promotes superior electrocatalytic activity for the prepared Ni₂P₂O₇ sample.
- The length and thickness of the Ni₂P₂O₇ were not significantly altered when compared to the as-prepared sample.

Ni₂P₂O₇ Microsheets for Water Splitting

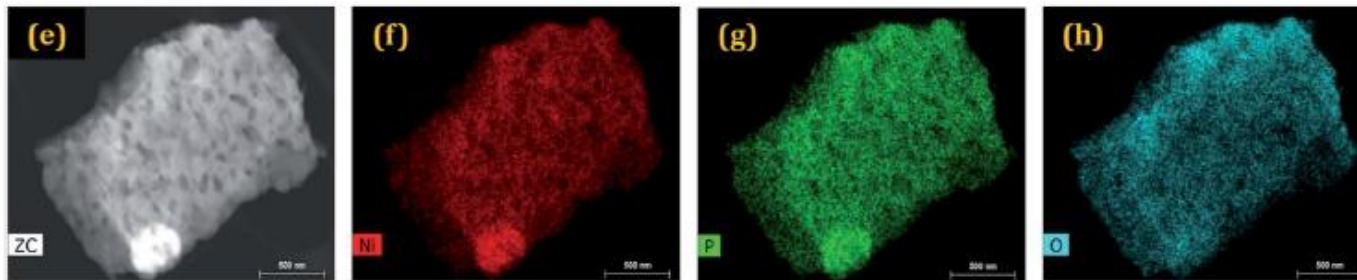
Sustainable Energy Fuels, 2019,3, 2435-2446

➤ High-Resolution Transmission Electron Microscopy (HRTEM) images



- HRTEM images shown in Fig. (a and b) confirm the creation of uniform circulated spongy porous microsheets of Ni₂P₂O₇ with a high surface roughness.
- The HRTEM image with the lattice fringes of the Ni₂P₂O₇ sample in Fig. (c) exhibits an interplanar spacing value of 0.22 nm, which corresponds with the high-intensity plane (112) of the monoclinic Ni₂P₂O₇ crystal structure.
- The SAED pattern shown in Fig. (d) clarifies that the prepared Ni₂P₂O₇ microsheets exist in the form of polycrystalline structures.

➤ Elemental mapping images



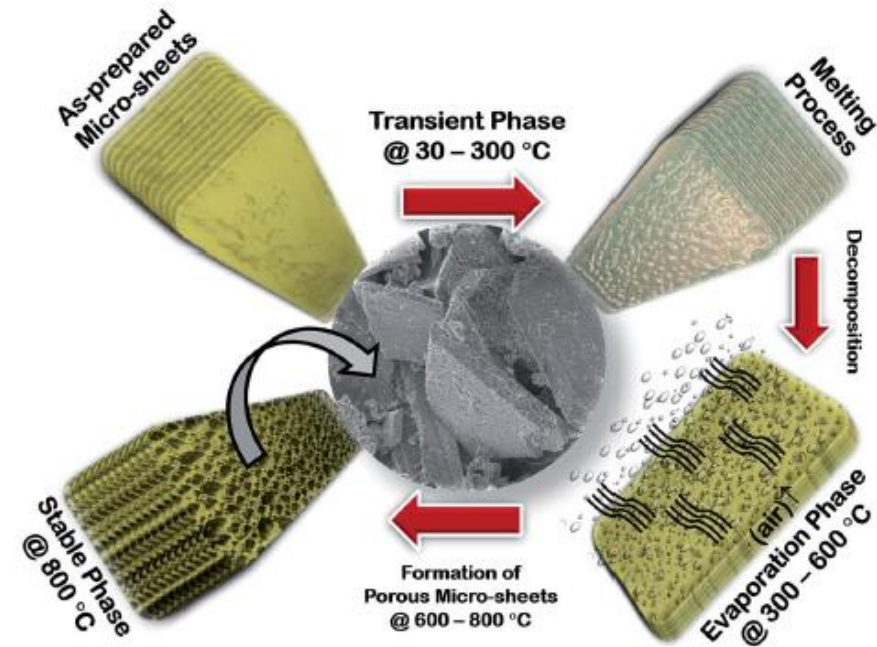
- Fig. (e–h) show the elemental mapping images of Ni₂P₂O₇, which validate the equivalently dispersed composition of Ni (red), P (green), and O (cyan) elements.

- Hence, the structural and morphological investigation dominantly authenticates that the Ni₂P₂O₇ sample was successfully synthesized and has potential for electrocatalytic activity.

Ni₂P₂O₇ Microsheets for Water Splitting

Sustainable Energy Fuels, 2019,3, 2435-2446

➤ Formation mechanism of porous spongy Ni₂P₂O₇ microsheets



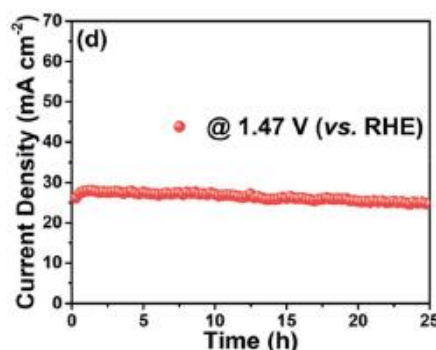
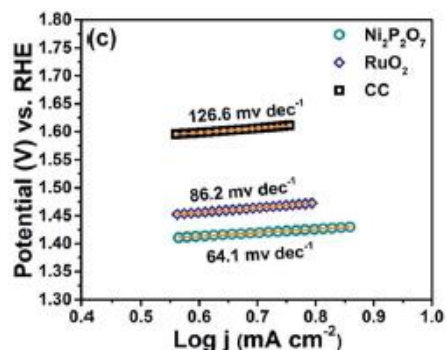
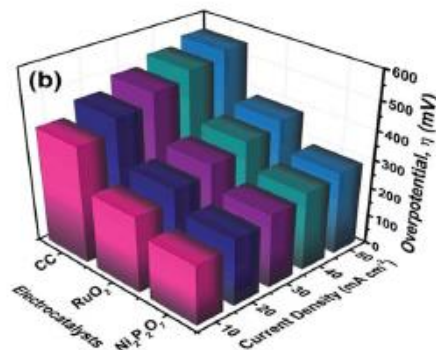
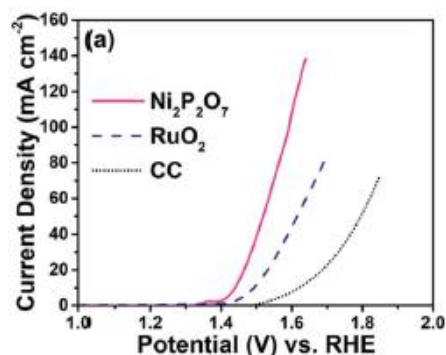
- During hydrothermal reaction, solid microsheets of NiNH₄PO₄·H₂O complex was obtained.
- Obtained solid microsheets were subjected to thermal treatment (800 °C) under an N₂ atmosphere, and porous, spongy Ni₂P₂O₇ microsheets were formed.
- The formation of these porous structures is explained based on the TGA analysis, where four conceivable phases occurred, namely, the transient period, melting step, evaporation phase, and stable phase.
- In the initial phase (25 to 200 °C), i.e., the temporary period, the imposed heat was well resisted by the solid microsheets of the NiNH₄PO₄·H₂O complex.

- Upon increase in the temperature, the complex microsheets started to melt deliberately as the unstable composition reached its melting point (200 °C to 300 °C).
- With a further increase in temperature, the volatile compositions in the complex reached their boiling point (300 °C to 600 °C) and began to evaporate.
- This evaporation phase resulted in a steep weight loss of about 30% of the as prepared complex.
- As a result of this evaporation phase, the unstable compositions present in the plane microsheets became detached, creating abundant pores and roughness on the surface.
- This phase initiated the formation of an aggregated **spongy, porous structure** on the Ni₂P₂O₇ surface.

Ni₂P₂O₇ Microsheets for Water Splitting

Sustainable Energy Fuels, 2019,3, 2435-2446

➤ OER Electrochemical properties of the Ni₂P₂O₇ electrodes



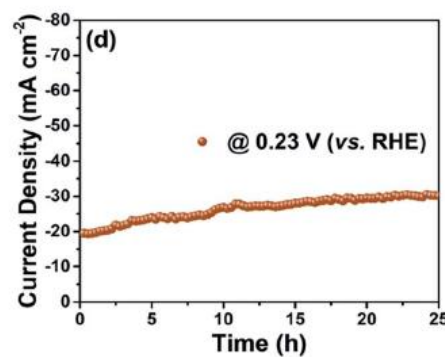
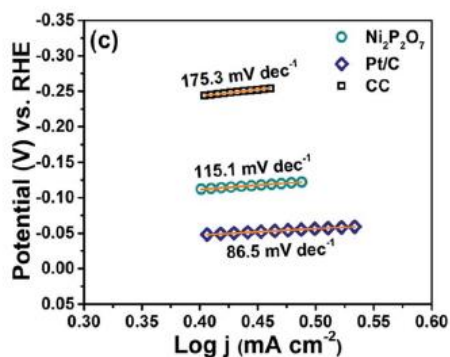
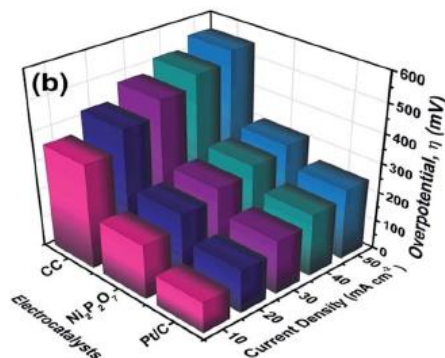
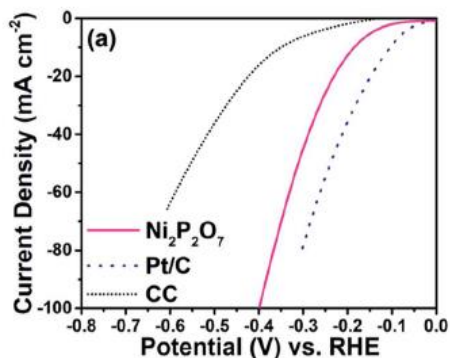
- Fig. (a) shows the OER polarization curves of Ni₂P₂O₇ together with that of the state-of-the-art RuO₂ electrocatalyst and bare commercial carbon cloth (CC) substrate.
- The curve shows a minor peak at 1.35 V (vs. RHE), which indicates the oxidation of the active Ni species (Ni²⁺/Ni³⁺) in the electrocatalysts.
- Ni₂P₂O₇ microsheets were found to be a superior electrocatalyst than RuO₂ and CC, yielding the operative onset potential at 1.39 V (vs. RHE).
- Ni₂P₂O₇ microsheets required an interestingly lower overpotential of 210 mV to reach an initial current density of 10 mA cm⁻² than the commercial RuO₂ electrocatalyst ($\eta_{10} = 263$) and CC ($\eta_{10} = 405$).

- The required OER overpotentials demanded by all three electrodes with respect to the acquired current densities (10 to 50 mA cm²) are portrayed in Fig. (b).
- In addition, the Tafel plot was obtained to identify the rate determining step in the oxygen evolution reaction (Fig. (c)).
- Fig. (d) displays the CA curves of the Ni₂P₂O₇ electrocatalyst at an applied potential of 1.47 V (vs. RHE) for 25h.
- The steady-state CA curve acquired by the Ni₂P₂O₇ microsheets ensures the resilient durability of the electrocatalyst for efficient and durable OER activity.

Ni₂P₂O₇ Microsheets for Water Splitting

Sustainable Energy Fuels, 2019,3, 2435-2446

HER Electrochemical properties of the Ni₂P₂O₇ electrodes



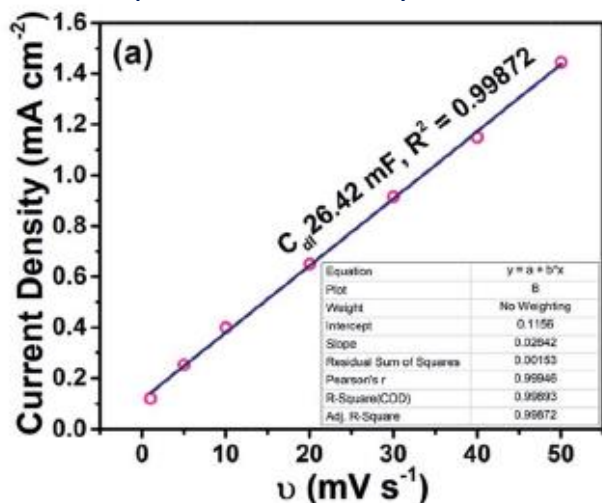
- The HER polarization curves in Fig. (a) show that the prepared Ni₂P₂O₇ microsheets responded with a significant onset potential at 0.09 V (vs. RHE).
- Ni₂P₂O₇ as an active electrocatalyst requires a minimal overpotential of 185 mV to reach a primary current density of 10 mA cm⁻².
- In contrast, the commercial Pt/C (104 mV) electrocatalyst requires a reasonably equivalent overpotential to reach the same current density.
- The required HER overpotentials demanded by all three electrodes with respect to the acquired current densities (10 to 50 mA cm⁻²) are portrayed in Fig. (b).
- Fig. (c) shows the obtained Tafel plots of the corresponding HER activity of the Ni₂P₂O₇ microsheets.

- Similar to the OER activity, the slightly oxidized Ni^{III} state of the Ni element acted as the highly active sites for HER.
- Using first principle calculations, Dong et al. reported that the slightly oxidized Ni atoms, not Ni⁰ atoms, are only responsible for the superior HER activity of Ni-based electrocatalysts as active sites.
- Hence, the oxidized Ni^{III} active centres shielded by the P species are the active sites for the OER and HER catalytic activities in the present case.

Ni₂P₂O₇ Microsheets for Water Splitting

Sustainable Energy Fuels, 2019,3, 2435-2446

➤ Linear plots of double layer current as a function of scan rate, LSV curves for OER activity



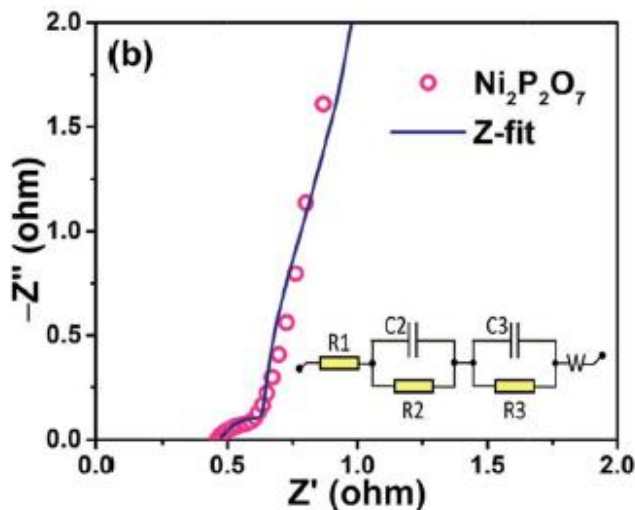
- The measured current densities in contrast to the scan rates were fitted linearly to acquire the respective C_{dl} from the equation below (Fig. (a)).

$$i_c = v \times C_{dl}$$

- where, i_c and v are the charging current and scan rate, respectively.
- The C_{dl} of the Ni₂P₂O₇ electrocatalyst was calculated to be 26.7 mF cm⁻² with a corresponding R^2 value of 0.99872.
- From the obtained double-layer capacitance value, the ECSA was calculated using eqn(2),

$$ECSA = C_{dl}/C_s$$

➤ Nyquist plots of Ni₂P₂O₇

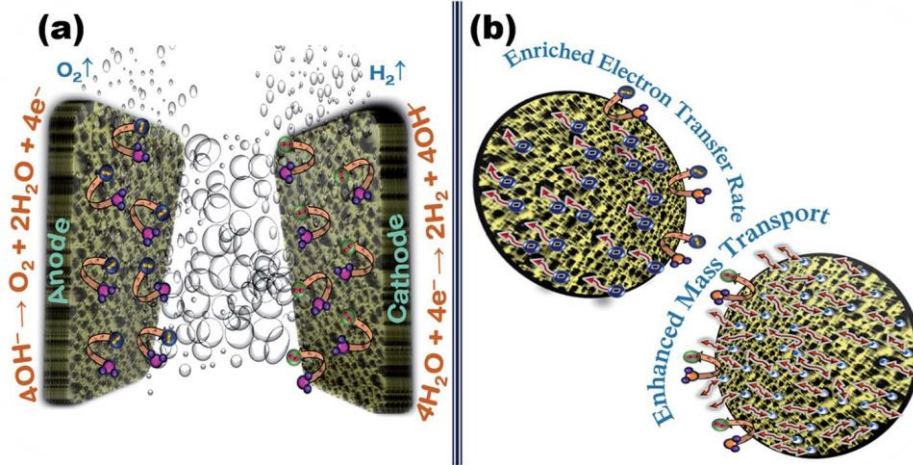


- where, C_s is the capacitance of the material with an atomically smooth surface per unit area obtained at identical electrolytic conditions.
- The estimated values were around 0.04 mF cm² in 1 M KOH electrolyte.
- Thus, the ECSA of Ni₂P₂O₇ was calculated to be 667.5 cm².
- Fig. (b) shows the EIS spectra fitted with an equivalent circuit to obtain the charge transfer resistance (R_{ct}) value of the Ni₂P₂O₇ microsheets.

Ni₂P₂O₇ Microsheets for Water Splitting

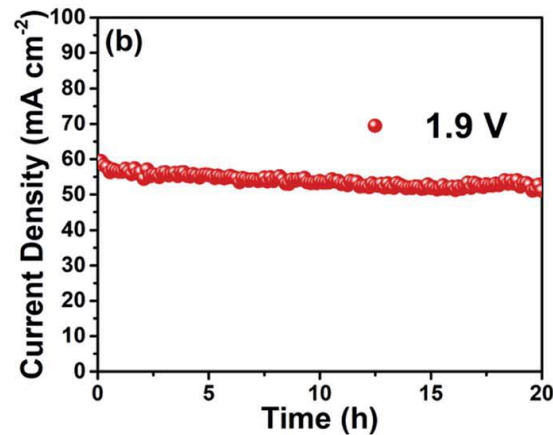
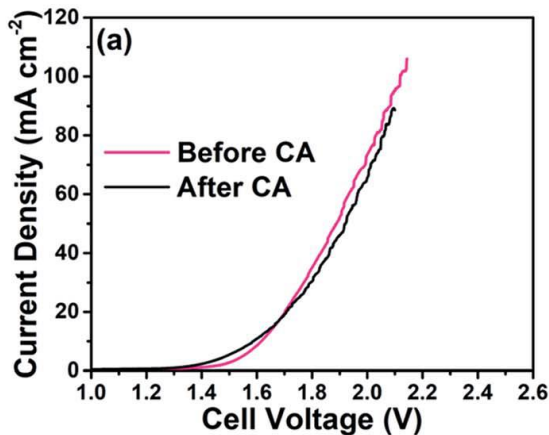
Sustainable Energy Fuels, 2019,3, 2435-2446

- Model of the faricated water splitting system and mass transfer rate



- Owing to the superior bi-functional electrocatalytic ability of the prepared Ni₂P₂O₇ microsheets, a lab-scale water electrolyzer was fabricated, as shown in Scheme (a).
- The porous morphology dominated the bi-functional electrocatalytic activity of the prepared Ni₂P₂O₇ microsheets, as illustrated in Scheme (b).

- Linear plots of double layer current as a function of scan rate, LSV curves for OER activity



- The CA analysis (Fig. (b)) to evaluate the durability of the formulated water electrolyzer was performed at a fixed applied cell potential of 1.9V.

- The assembled water electrolyzer exhibited a nominal cell potential of 1.61 V to establish an improved water-splitting current density of 10 mA cm⁻², resulting in the mammoth discharge of huge volumes of O₂ and H₂ gas bubbles from the surfaces of the anode and cathode, respectively.

Hydrothermal deposition of CoS nanostructures and its multifunctional applications in supercapattery and water electrolyzer

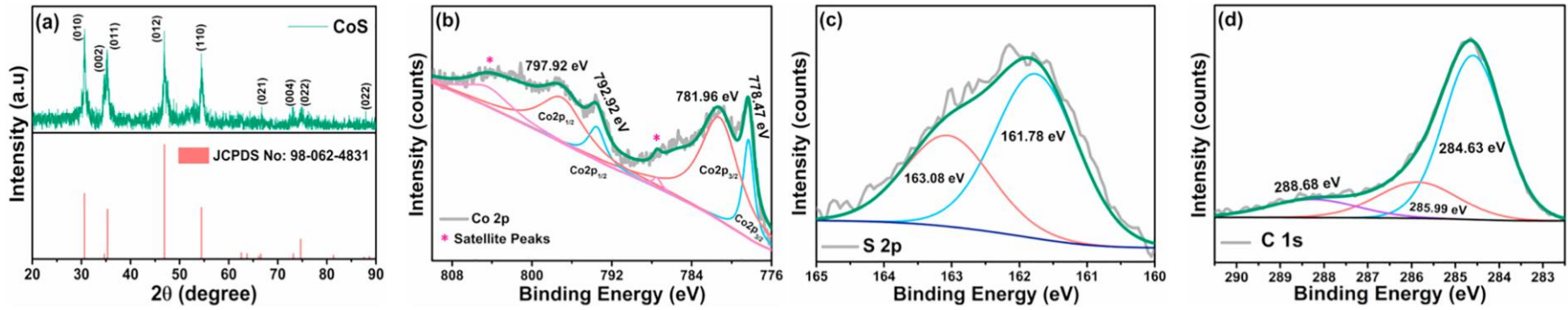
Published

Subramani Surendran^{a,b,*}, Sathyanarayanan Shanmugapriya^a,
Harivignesh Ramasamy^c, Gnanaprakasam Janani^b, Dharmalingam
Kalpana^d, Yun Sung Lee^c, Uk Sim^{b,**}, Ramakrishnan Kalai Selvan^{a,**}

CoS@CC for Water Splitting

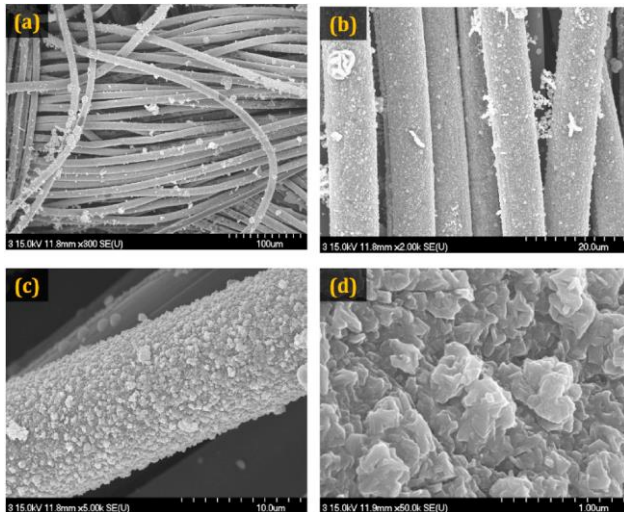
➤ XRD pattern & XPS spectra

Applied Surface Science 494 (2019) 916–928



- Fig. (a) shows the strong peaks at 32° and 48° was precisely associated to the (010) and (012) lattice planes.
- Fig. (b) was deconvoluted into six significant components, where the Co $2p_{3/2}$ part at lower binding energies includes three integrant.
- In Fig. (c), The two broad peaks at around 163.08 eV ($S 2p_{1/2}$) and 161.78 eV ($S 2p_{3/2}$) can be attributed to the sulfur-metal bonds in Co-S and S_2^- in low coordination on the surface, respectively.

➤ FESEM images of flake-like CoS

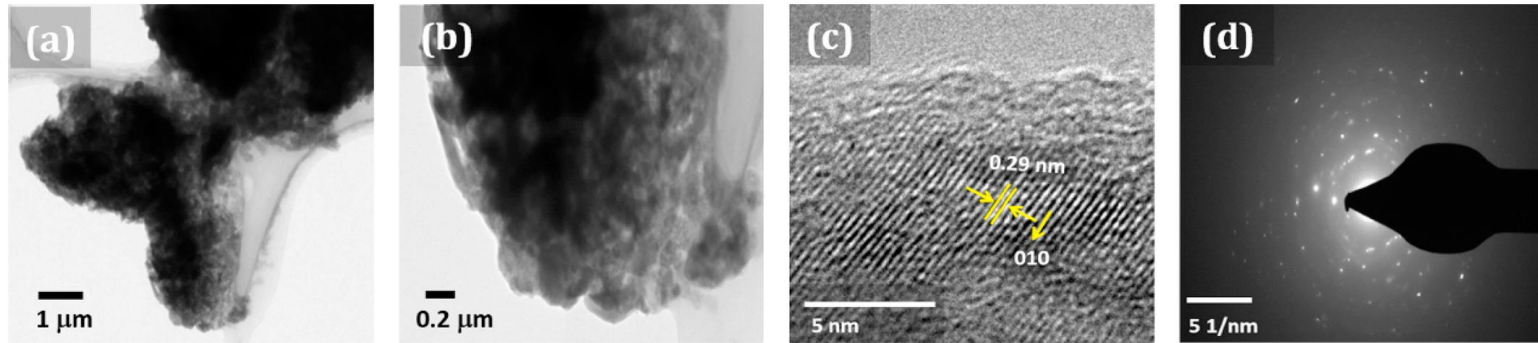


- The FESEM images displays the morphological properties of the in-situ grown CoS particles over the carbon cloth.
- A well-defined, meticulously packed arrangement of flake-like CoS nanostructures on CC was formed, as shown in Fig. (a–d).
- The average size of the individual flakes was measured to be around $0.33 \mu\text{m}$.
- As a result, a well-aligned, uniform flake-like CoS were widely erected over the carbon cloth.

CoS@CC for Water Splitting

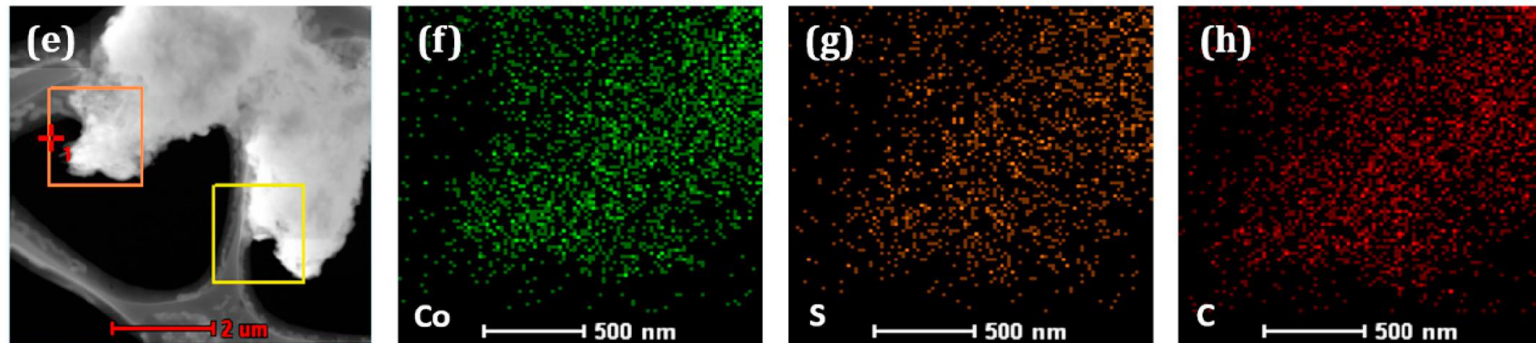
Applied Surface Science 494 (2019) 916–928

➤ TEM images, HRTEM images, SAED pattern



- The HRTEM images in Fig. © show distinct lattice fringes with interplanar distances of 0.29 nm corresponding to the (010) plane of the CoS crystal structure.
- Fig. (d) portrays the SAED pattern that illustrates the polycrystalline nature of the prepared sample.
- This elucidates that the prepared CoS is in good agreement with the obtained XRD pattern.

➤ Elemental mapping images

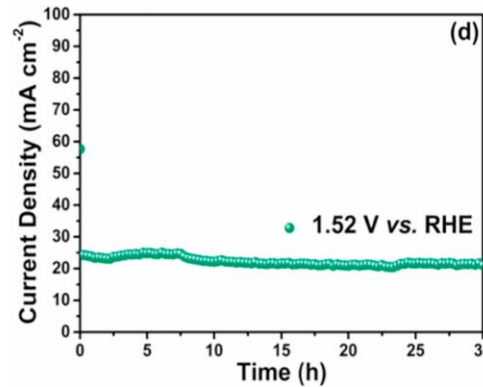
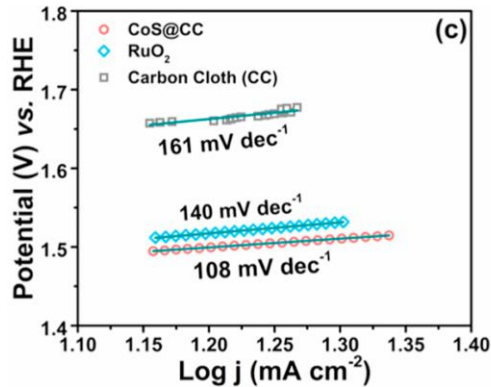
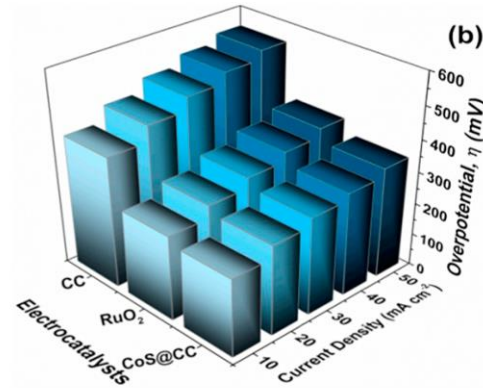
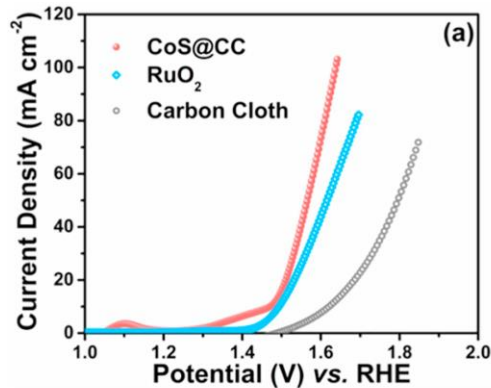


- The elemental mapping images of CoS are shown in Fig. (e–h), which confirms that the Co, S, and C elements were uniformly distributed in the prepared sample.

CoS@CC for Water Splitting

Applied Surface Science 494 (2019) 916–928

➤ Oxygen evolution Reaction



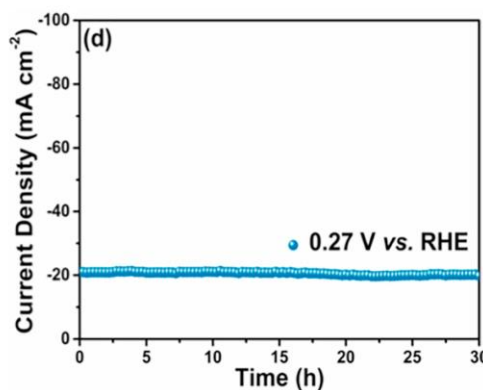
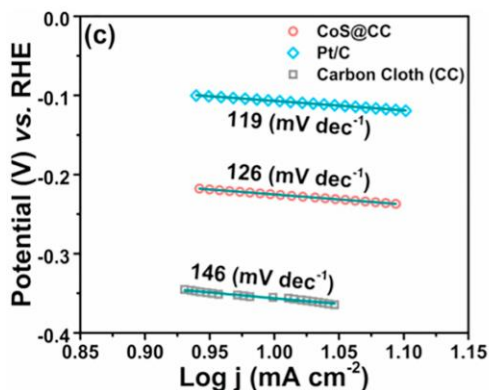
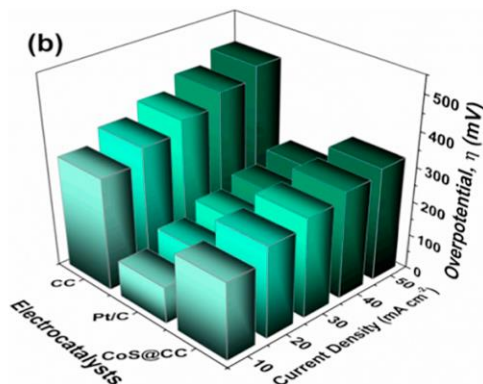
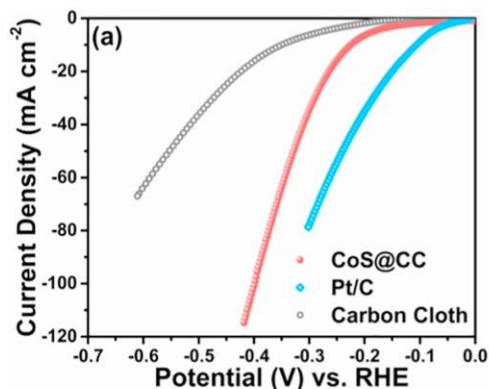
- Fig. (a) shows a sharp peak at 1.1 V (vs. RHE) and a broader peak at 1.4 V (vs. RHE) owing to the oxidation reactions associated to the Co²⁺/Co³⁺ and Co³⁺/Co⁴⁺ redox couples, respectively.
- Fig. (b) exemplifies the essential OER overpotentials of the electrocatalysts to reach different current densities (10 to 50 mA cm⁻²).
- Tafel slopes of CoS, RuO₂ and CC OER electrocatalyst are presented in Fig. (c).
- Electrocatalytic activity of CoS electrocatalyst was engrossed by a single electron transfer step with a minimum Tafel slope of 108 mV dec⁻¹.

- The overall OER catalytic activity of the CoS@CC electrocatalysts can be accredited to the active Co species in the sulfide.
- Besides, the flake-like arrangement of CoS nanostructures on CC relish with a superior surface roughness that creates more active sites enhancing the efficiency of the OER activity

CoS@CC for Water Splitting

Applied Surface Science 494 (2019) 916–928

➤ Hydrogen evolution Reaction



- Fig. (a) shows that the flake-like CoS electrocatalyst grown over the CC shows an exceptional catalytic activity by initiating an onset potential at **0.156 V** (vs. RHE).
- The prepared CoS electrocatalyst requests an overpotential of **264 mV** to accomplish an eminent current density of **20 mA cm⁻²**.
- Fig. (b) exemplifies the essential HER overpotentials for the electrocatalysts to reach different intervals of current densities (10 to 50 mA cm⁻²).
- CoS@CC requisites a low overpotential of **327 mV** to accomplish an improved current density (**50 mA cm⁻²**) ensuring a better catalytic activity even at the applied high potential value.

• The rate determining step of CoS electrocatalyst for HER catalytic activity is obtained from the Tafel analysis (Fig. (c)).

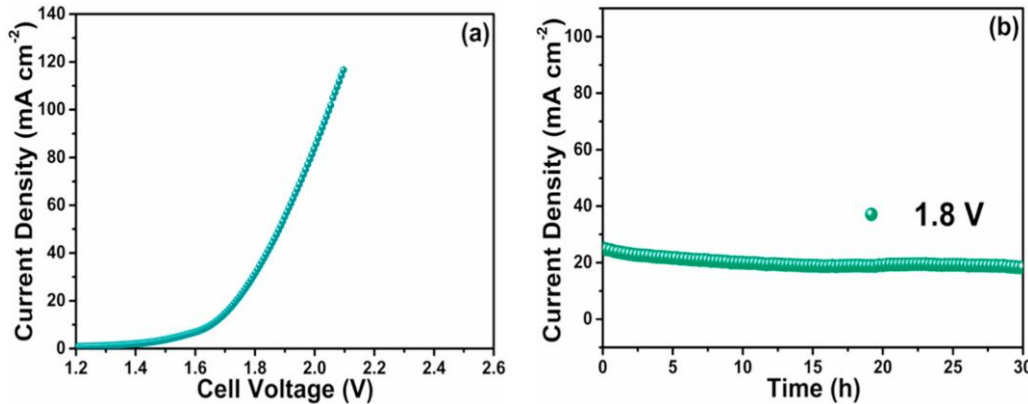
• The CA analysis (Fig. (d)) carried out with a steady potential of -0.27 V (vs. RHE) for 30 h witnesses an eminent strength towards the durability of the CoS@CC electrocatalyst with a nearly constant current and continuous evolution of gas bubbles all through the CA analysis.



CoS@CC for Water Splitting

Applied Surface Science 494 (2019) 916–928

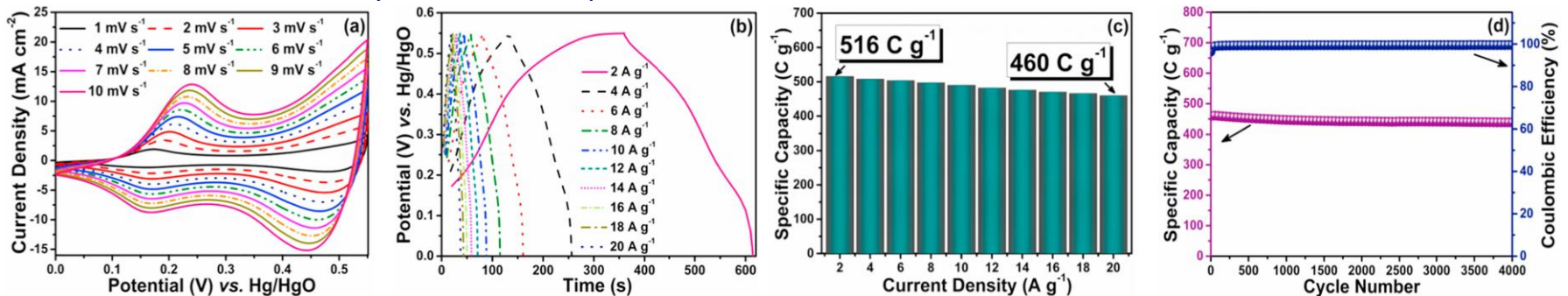
➤ Fabrication of lab-scale water splitting system



- From the respective LSV curve of the designed flexible water-splitting system (Fig. a), significant water splitting current density of 10 mA cm^{-2} was achieved with a nominal cell potential of 1.65 V .

- The CA analysis (Fig. b) of the assembled water-splitting system provides a stable trajectory inducing the resilient bifunctional activity of the CoS@CC electrodes at a persistent cell potential of 1.80 V for 30 h.

➤ Electrochemical activity of CoS@CC as positrode



- (a) CV curves of CoS@CC electrode at different scan rates, (b) GCD curves of CoS@CC electrode at different current densities, (c) current density with respect to the specific capacity plot of the CoS@CC electrode, and (d) cycling stability curve of the CoS@CC electrode for 4000 cycles.